Silver Nanoparticles as Dual Sensors for Selective Detection of Hexavalent Chromium and Cyanide Ions

María del Carmen Aguirre[1*], Paula G. Bercoff [1,2]

[1]Instituto de Física Enrique Gaviola (IFEG), Conicet. Ciudad Universitaria, 5000 Córdoba, Argentina.
[2]Facultad de Matemática, Astronomía, Física y Computación. Universidad Nacional de Córdoba. Ciudad Universitaria, 5000 Córdoba, Argentina.
* Corresponding author e-mail: maria.aguirre@unc.edu.ar

Abstract

Silver nanoparticles stabilized in starch (AgNPs@starch), were synthesized via chemical reduction, yielding spherical nanostructures with an average diameter of (5 ± 1) nm. The surface plasmon resonance (SPR) band at 400 nm served as the analytical signal for the colorimetric detection of hexavalent chromium [Cr(VI)] and cyanide (CN^-) ions under various aqueous conditions. Cr(VI) detection was conducted using AgNPs@starch at pH 2, 4 and acetate buffer at pH 4.75 (ABS pH 4.75), in the presence of ethylenediaminetetraacetic acid (EDTA) as a stabilizer. Although slightly higher sensitivity was observed in unbuffered systems at pH 4, the buffered environment ensured improved nanoparticle stability and extended the detection range (0-100 µM) without compromising the limit of detection (LOD) of 0.2 µM. The use of the pH 4.75 buffer reduced oxidative degradation of AgNPs, preserving optical performance and reducing the rate of absorbance decrease upon Cr(VI) addition compared to unbuffered media. Analysis of real water samples (coming from Suquía River in Córdoba, Argentina) and common interferents confirmed the selectivity and sensitivity of the nanosensor under both buffered and unbuffered conditions.
Cyanide was also selectively and rapidly detected using AgNPs@starch in borate buffer at pH 8.4 (BBS pH 8.4), achieving an LOD of 0.24 µM over a concentration range 0-85 µM. The AgNPs@starch sensor maintained excellent analytical performance in the presence of common interferents (Ca^{2+}, Mg^{2+}, halides) and in real water samples, with calibration curves exhibiting relative errors below 5% compared to pure systems.

Graphical Abstract

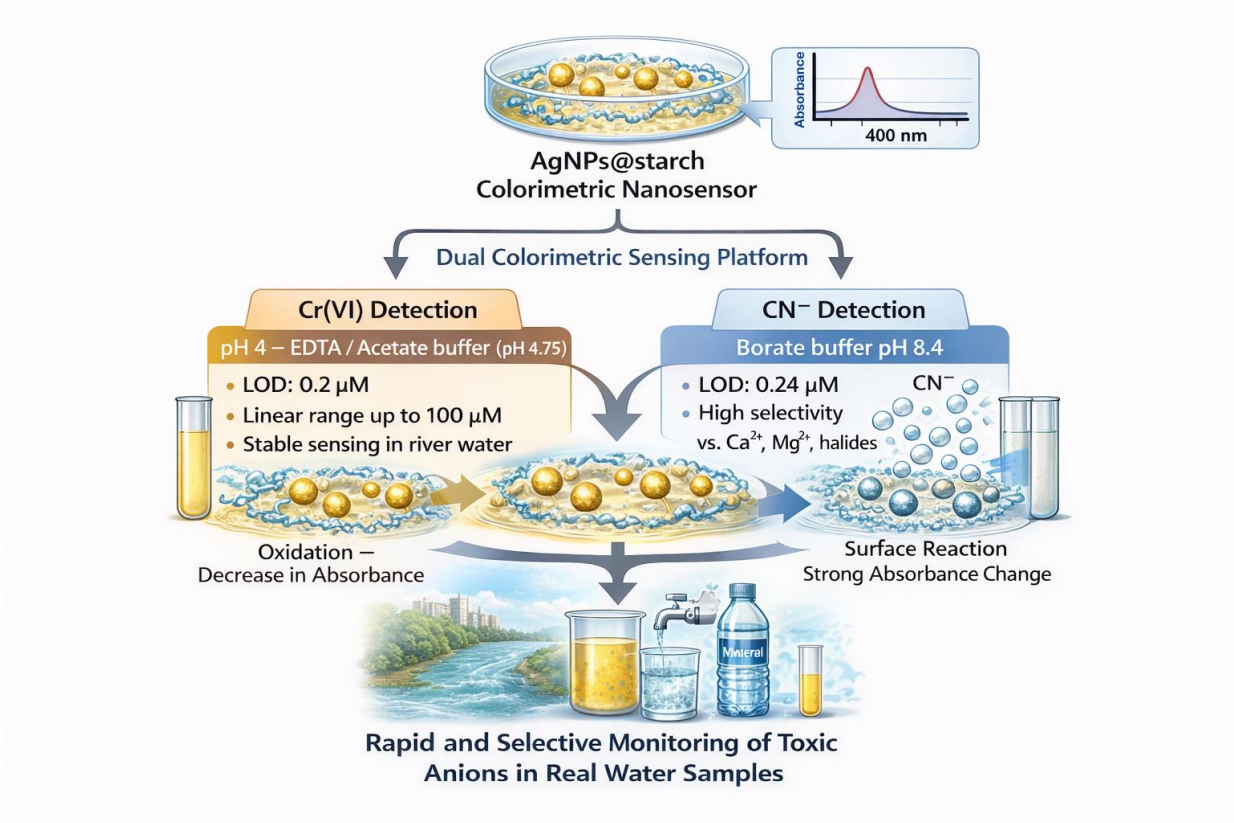

1. Introduction

Organic pollutants include herbicides such as glyphosate, industrial chemicals, and by-products of industrial processes such as hexavalent chromium and cyanide. Among these contaminants, anionic species are of particular concern due to their high stability and complex biodegradation pathways. In particular, chromate and cyanide are of great toxicological interest. Cyanide is commonly found in leaching solutions from gold and silver metallurgy, in metal plating, tanning processes, and in certain wastewaters [1–6].

From a toxicological perspective, cyanide poses serious health risks. It binds to essential iron-containing enzymes, impairing cellular oxygen utilization and leading to brain hypoxia [2]. According to the U.S. Environmental Protection Agency (EPA), cyanide is lethal to humans at doses of 0.5-3.5 mg per kg of body weight, and the maximum contaminant level goal (MCLG) in drinking water is set at 0.2 mg/L [3]. This concentration is not expected to cause adverse health effects. In 2015, the EPA revised the ambient water quality criterion for cyanide, requiring public water supplies (PWS) to maintain total cyanide concentrations below 4 µg/L [4]. However, untreated surface water rarely meets this standard and thus is generally unsuitable for direct distribution.

Hexavalent chromium [Cr(VI)] has been classified by the EPA as a Group A human carcinogen, associated with lung and sinonasal cancers. The World Health Organization (WHO) has established a guideline value of 50 ppb for total chromium, including Cr(VI), in groundwater [5].

Nanomaterials have gained significant attention as colorimetric sensors [6-21]. Metallic nanoparticles, particularly those of silver, cobalt, and gold, are widely employed as optical probes for detecting organophosphate pesticides, heavy metals, and other toxic compounds [9-13]. The application of silver nanoparticles (AgNPs) for colorimetric detection of Cr(VI) and cyanide in water has been reported [2,7,8,14-23]. However, few studies have investigated the potential interference caused by chromate coloration during detection, or the influence of the dispersing medium used to stabilize AgNPs. Furthermore, there are no reports on the performance of AgNPs for Cr(VI) detection in both unbuffered and buffered solution at similar pH values.

In the present work, starch was selected as the capping and stabilizing agent for AgNPs, owing to its ability to prevent nanoparticle aggregation over extended periods. This property contrasts with that observed for AgNPs capped with ascorbic acid or raffinose [16,19], where the reduction products of Cr(VI), such as Cr(III), can coordinate with OH^- groups on the NP surface, promoting aggregation. Moreover, silver nanoparticles stabilized in a starch solution (AgNPs@starch) were evaluated as a sensing platform for the colorimetric detection of cyanide. To the best of our knowledge, this approach has not been previously reported. Compared to other AgNP-based sensors, the platform demonstrated a shorter analysis time by eliminating the need for a lengthy incubation step. Additionally, it enabled an extended linear detection range for cyanide when tested in real aqueous systems.

Real water samples, such as those from industrial effluents, mining leachates, and surface waters, present complex matrices with varying ionic strengths, organic matter, and co-existing interferents that can compromise sensor reliability in controlled lab settings. Routine monitoring of Cr(VI) and cyanide in these environments is essential for compliance with stringent EPA and WHO regulations, yet conventional methods like chromatography or spectroscopy often require expensive equipment, skilled operators, and lengthy sample preparation. Thus, validating AgNPs@starch in untreated real water samples is critical to demonstrate its robustness, selectivity, and field-deployability, enabling rapid on-site assessment to mitigate health risks from contaminated water sources in high-risk areas like mining regions.

UV-Vis spectroscopy is a powerful tool for characterizing AgNPs, as it provides information on nanoparticle size and morphology through their characteristic surface plasmon resonance (SPR) absorption maxima, typically ranging from 391 to 453 nm [6,7,14,16,18-27]. A shift of the SPR band toward shorter wavelengths indicates the formation of smaller nanoparticles, reflecting the strong size dependence of their optical and electronic properties [7,27]. For example, Raveendran et al. [24] synthesized AgNPs using β-glucose, stabilizing them in aqueous starch dispersions, with an SPR maximum at 419 nm. Similarly, starch-stabilized AgNPs prepared following Wongravee et al. [14,25] displayed a dipolar SPR peak at 400 nm, attributed to spherical morphology. Amirjani et al. [26] further demonstrated that Ag nanostructure geometry strongly influences optical behavior: silver nanotriangles (~30 nm edge) exhibited absorption near 650 nm, while silver nanospheres (60 nm diameter) showed a peak around 400 nm.

Here, we report the synthesis by chemical reduction, of spherical, highly monodisperse silver nanoparticles stabilized in starch solution (AgNPs@starch). The resulting colloid, characterized by a sharp SPR band at 400 nm, was employed as a colorimetric sensor for cyanide and Cr(VI) detection. The system was tested under different conditions: cyanide at pH 8.4, and Cr(VI) at pH 2, pH 4, and in a sodium acetate/acetic acid buffer at pH 4.75 ─a combination not previously reported. The selectivity of AgNPs@starch toward Cr(VI) and cyanide was further evaluated in the presence of potential interferents (various anions and cations) and in real water samples. Upon increasing concentrations of cyanide or Cr(VI), the characteristic SPR band at 400 nm progressively decreased. For both analytes, detection (LOD) and quantification (LOQ) limits were determined. Overall, AgNPs@starch provide a simple, rapid, and sensitive platform for detecting Cr(VI) and cyanide, with performance comparable or superior to other nanoparticle-based systems, while remaining practical for routine water monitoring.

2. Experimental

The reagents and solutions used in all the experiments are described in the *Supplementary Information*. Starch-stabilized AgNPs (AgNPs@starch) were synthesized according to references [14,25] with small modifications. The starch solution at 1% (w/v) was prepared by adding 1 g of starch in boiling water and leaving to boil during 30 min. After the starch is well dissolved, it is left to cool at room temperature (≤23°C) and levelled to 50 mL with deionized (DI) water. Then, 31.5 mg $AgNO_3$ and 10.5 mg $NaBH_4$ are dissolved separately, each one with 25 mL of the starch solution. The $NaBH_4$/starch solution is put in an Erlenmeyer under stirring and then the $AgNO_3$/starch solution is added quickly to the borohydride solution, with vigorous stirring. The final solution changes from colourless to dark brown. Then, the volume is increased to 90 mL with DI water, and it is stirred for 30 min at room temperature (≤23°C). After that, the temperature is increased up to boiling point. The synthesized AgNPs colloid is gently boiled while stirring for 2 h to eliminate any residual product from borohydride. After that, the solution is cooled down to room temperature. The as-prepared solution was adjusted to 100 mL with ultrapure water and incubated at room temperature overnight. The nominal concentration of silver nanoparticle suspension is 1.85 mM; ICP-MS confirmed the Ag content in the colloid. The as-prepared AgNPs suspension was stable for several months at room temperature, without any aggregation or colour changes.

UV-Vis measurements were performed using a UV-Vis spectrophotometer Lambda 365 (Perkin Elmer). The spectra were recorded at room temperature using a 1.0 cm path length of quartz cells. The wavelength range used for measuring the absorbance is from 200 nm to 700 nm. AgNPs@starch were stable for approximately 3-4 months.

As mentioned in the *Supplementary Information*, for our experiments five different kinds of waters were used: Deionized (DI), tap water (TW) from the southern water provision plant of Córdoba city (Argentina), two commercial brands of spring natural mineral water, with weak mineralization (NMW-1 and NMW-2) and contaminated water from the Suquía River(in Córdoba, Argentina) taken from the eastern margin, where the river receives the sewage discharge from the Municipal waste water treatment plant (WWTP). For further details regarding the composition, refer to the Supplementary Information.

A Sigma Zeiss Field Emission-Scanning Electron Microscope (FE-SEM), with an Oxford Energy Dispersive Spectrometer (EDS) was used to determine the samples' morphology and nominal chemical composition.

X-ray Photoelectron Spectroscopy (XPS) was used to determine surface composition of silver nanoparticles with a Thermo Scientific K-alpha equipment. Photoelectrons were excited with a source of monocromated, microfocused Al K-alpha radiation. A spot size of 400 µm and 35 scans were used in the measurements, with beam energy of 50.0 eV and energy step size of 0.01 eV. The binding energy of Ag $3d_{5/2}$ and Ag $3d_{3/2}$ was corrected considering the charge shift observed for the C 1s peak, that should be centered at 284.7 eV.

3. Results and Discussion

3.1 *Characterization of AgNPs*

Figure 1a shows the UV-Vis spectrum of 36 µM AgNPs stabilized in starch solution (AgNPs@starch) in the presence of 19 µM ethylenediaminetetraacetic acid (EDTA). EDTA was employed as a masking agent to eliminate the interfering effects of heavy metal cations without suppressing the analyte response [14]. The absorbance maximum was investigated over the wavelength range of 200 to 700 nm.

Figure 1a compares the spectra of freshly prepared and two-month-aged AgNPs@starch samples. Both spectra exhibit a narrow and intense absorption band with a maximum at 400 nm. The spectra are superimposable, indicating that starch effectively stabilizes the nanoparticles. The localized surface plasmon resonance (LSPR) band at 400 nm corresponds to the collective oscillation of free electrons in the conduction band of AgNPs, characteristic of predominantly spherical nanosized silver particles with a narrow size distribution [25-27]. The stability of AgNPs@starch was evaluated by storing the samples in dark at room temperature (25 °C) and pH 7, up to 120 days. The absorbance at 400 nm was monitored every 7 days to detect possible aggregation. No significant change (<1%) in absorbance was noticed during storage indicating the stability of silver nanoparticles. In Figures 1b - 1c, a representative TEM image and the corresponding particle size distribution histogram confirm that the AgNPs@starch are spherical with an average diameter of (5 ± 1) nm.

The surface oxidation state of silver was analyzed by X-ray photoelectron spectroscopy (XPS). A survey spectrum and core-level spectra for the Ag 3d (368-374 eV), C 1s (282-290 eV), and O 1s (528-536 eV) regions were systematically recorded (Figure 2a). From the Ag 3d core-level spectrum (Figure 2b), two peaks were observed at 368.04 eV and 374.16 eV, corresponding to Ag^0 $3d_{5/2}$ and Ag^0 $3d_{3/2}$, respectively. The C 1s peak at 284.79 eV was used as an energy reference (Figure 2c). In Figure 2d, the O 1s peak observed at 531.8 eV is attributed to hydroxyl-related species, likely due to water adsorption on the surface of AgNPs [28]. Contributions from silver oxides in the O 1s and C 1s regions were negligible.

These results confirm the reduction of Ag^+ to metallic Ag^0 by $NaBH_4$ using starch in the synthesis, which would act as a stabilizing agent. As previously reported for starch-coated gold nanoparticles [29], the hydroxyl-rich structure of the starch polymer can stabilize nanoparticles through electrostatic interactions involving oxygen atoms. Accordingly, it is proposed that starch molecules cap the AgNPs upon formation, thereby preventing aggregation and oxidation over time.

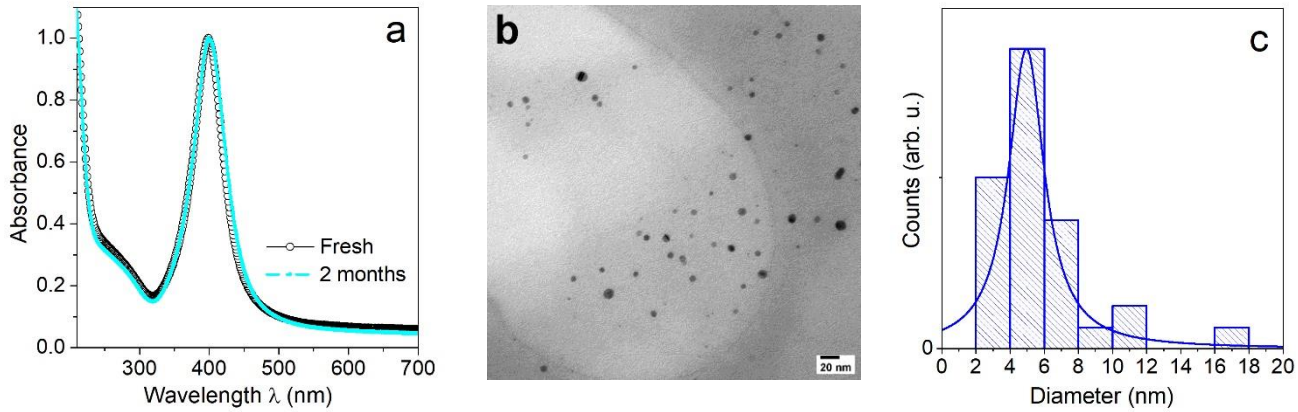

Figure 1. a) UV-Vis absorbance spectra of fresh and aged AgNPs@starch. b) TEM image of AgNPs@starch. c) Size histogram of AgNPs@starch.

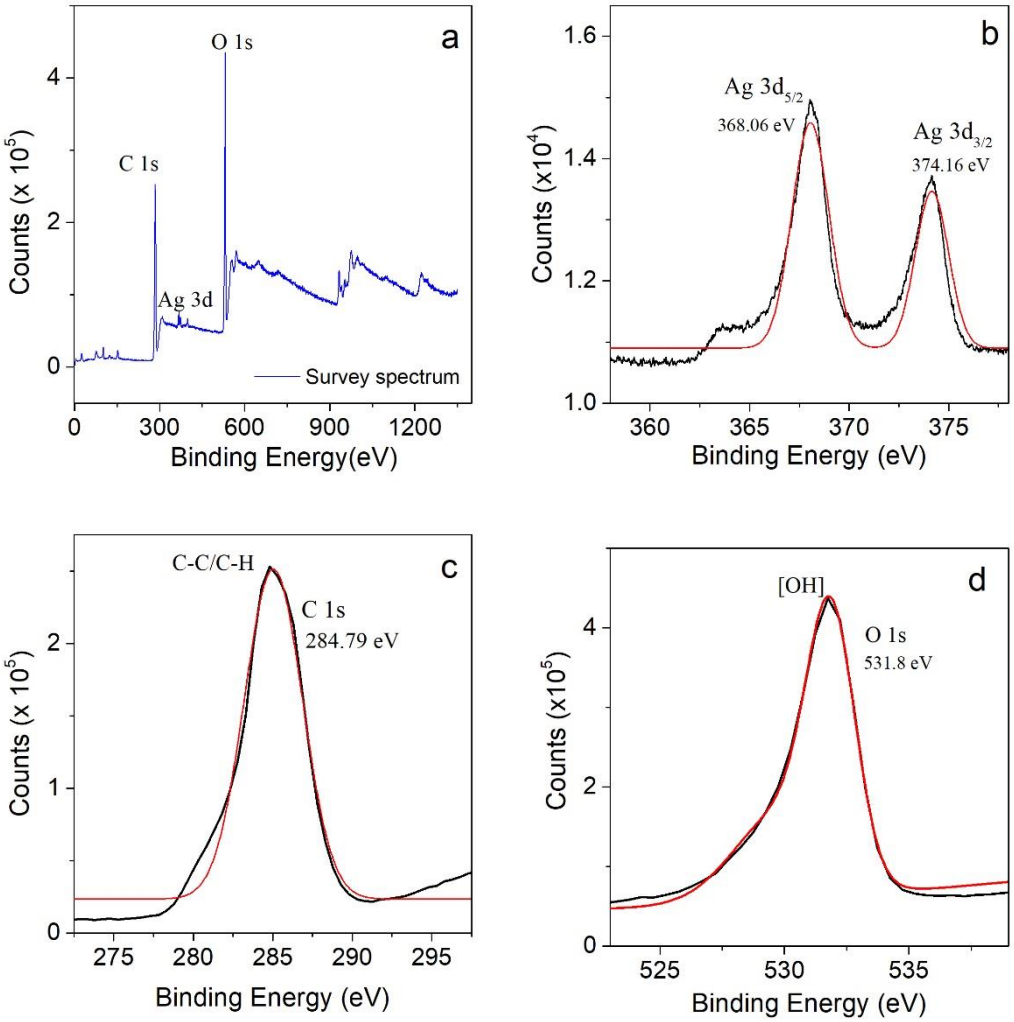

Figure 2. XPS measurements for AgNPs@starch. a) Survey spectrum, b) Ag 3d, c) C 1s, d) O 1s. The black line corresponds to the experimental data and the red line is the cumulative peak fit.

3.2 *Cr(VI) determination using AgNPs@starch as sensor*

The selective detection of hydrogen chromate anions ($HCrO_4^-$) by AgNPs@starch occurs under acidic conditions. The acid-base equilibria of chromic acid and its conjugate bases are defined by the pKa values of the $H_2CrO_4/HCrO_4^-$ ($pKa_1 = 0.75$) and $HCrO_4^-/CrO_4^{2-}$ ($pKa_2 = 6.4$) couples [30]. At the pH values investigated (pH 2, 4, and acetate-buffered solution at pH 4.75), Cr(VI) predominantly exists in the hydrogenated form ($HCrO_4^-$), whereas above pKa_2, the chromate ion (CrO_4^{2-}) becomes the major species. This shift in Cr(VI) speciation with pH is accompanied by a visible color change from light yellow to amber, corresponding to a red shift in the charge-transfer absorption band [30,31].

In the initial assay, a mixture of 36 µM freshly prepared AgNPs@starch and 19 µM EDTA in deionized (DI) water was placed in a quartz cuvette, and aliquots of Cr(VI) were added from a 5 mM stock solution. The UV-Vis spectra at pH 2 and pH 4 were recorded and are shown in Figures 3a and 3b, respectively. EDTA served to stabilize the AgNPs@starch signal by suppressing interference from other cations. The proposed mechanistic pathway for Cr(VI) reduction at the surface of AgNPs@starch in the presence of EDTA is explained in the Supplementary Information.

At pH 2 (Figure 3a), the AgNPs@starch displayed a stable absorption maximum at 400 nm, whose intensity decreased progressively with increasing Cr(VI) concentration (0-60 µM). This reduction indicates a strong interaction between Cr(VI) and the AgNP surface, likely displacing the starch capping layer. The decrease in absorbance at 400 nm is attributed to a redox reaction between $HCrO_4^-$ and metallic silver (Ag^0), whereby $HCrO_4^-$ acts as an oxidizing agent and the AgNPs are partially oxidized, resulting in diminished plasmonic response.

At higher Cr(VI) concentrations, a color change occurred in the AgNPs@starch colloid, accompanied by the emergence of two absorption bands at 348.25 nm and 256 nm, characteristic of the intrinsic charge-transfer transitions of chromate ions [7,29-34]. The intensities of these bands increased with Cr(VI) concentration in the range of 75-220 µM. The inset of Figure 3a shows the corresponding calibration curves at the three wavelengths. Linear relationships were obtained with correlation coefficients ($r^2 \geq 0.98$) and slopes of S(400 nm) = (-15 ± 1) × 10^{-3} μM^{-1}, S(348 nm) = (28 ± 3) × 10^{-4} μM^{-1}, and S(256 nm) = (39 ± 3) × 10^{-4} μM^{-1}. Remarkably, the response of AgNPs@starch was approximately an order of magnitude higher than the direct colorimetric signal of Cr(VI) (at 256 and 348 nm). Comparable behavior was observed at pH 4 (Figure 3b), yielding slopes of S(400 nm) = (-16 ± 1) x 10^{-3} μM^{-1}, S(348 nm) = (27 ± 3) × 10^{-4} μM^{-1}, and S(256 nm) = (36 ± 3) × 10^{-4} μM^{-1}.

Previous studies employing starch-stabilized AgNPs for Cr(VI) detection have generally been conducted under strongly acidic conditions (typically pH ≈ 3) [14], where oxidation of the nanoparticles produces a distinct visual color change, enabling detection. However, the present system demonstrates improved selectivity and lower detection limits, representing a significant advancement over previously reported approaches. Other reports [7,14-18,20] indicate that the optimal pH for Cr(VI) detection depends strongly on the nanoparticle capping agent. For example, He *et al.* achieved maximum response for polyvinylpyrrolidone (PVP)-functionalized AgNPs in phosphate buffer at pH 5.5 [20], whereas ascorbic acid-capped AgNPs required adjustment to pH 7.6 [16]. Similarly, another study [31] reported maximum absorbance at pH 2.2 using 1,5-diphenylcarbazide (DPC) as the colorimetric reagent.

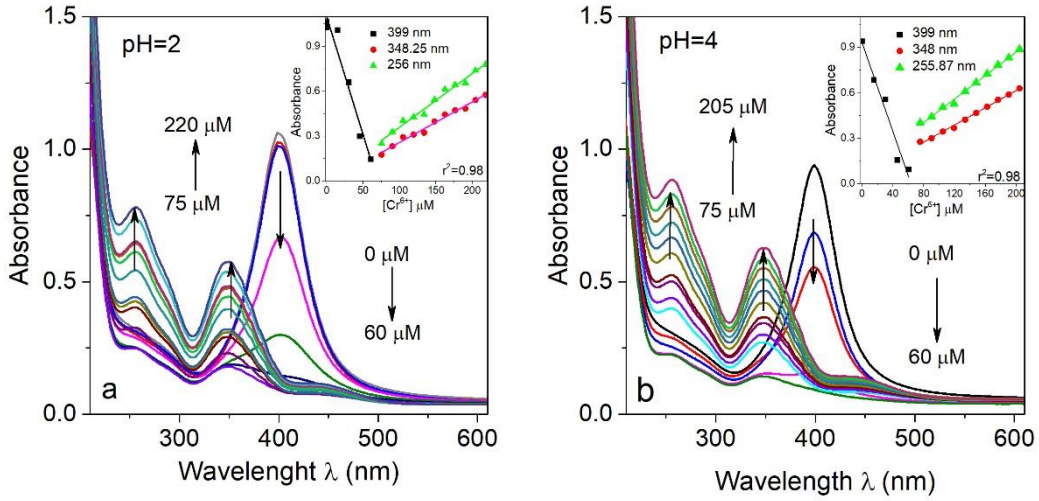

Figure 3. SPR spectra of 36 µM AgNPS@starch solution with 19 µM EDTA upon Cr(VI) addition. a) pH 2 b) pH 4. The insets correspond to the calibration curves.

In the present work, assays were carried out at pH 4 and in acetate buffer solution (ABS, pH 4.75) to balance nanoparticle stability with Cr(VI) reactivity, thereby promoting a selective sensing mechanism. Additional measurements exploiting the intrinsic chromate color were performed in different water matrices, including DI water, natural mineral water (NMW-2), tap water (TW) and Suquía River water, as described in the *Materials* section of the Supplementary Information. Direct Cr(VI) detection by UV-Vis spectroscopy at 348 nm and 256 nm allowed quantification in the 0-190 µM range, though sensitivity at low concentrations was substantially lower than that achieved with AgNPs@starch, confirming its superior efficiency.

To optimize sensor performance, the concentrations of AgNPs@starch and EDTA were varied to minimize direct Cr(VI) coloration and extend the linear detection range. The UV-Vis spectra for 57 µM AgNPs@starch with 48 µM EDTA at pH 4 and the corresponding calibration curve are shown in Figures 4a and 4b. Cr(VI) concentrations ranged from 0 to 84 µM (0, 9, 19, 28, 37, 47, 56, 65, 74, and 84 µM). The plasmon band remained narrow and centered at 400 nm, indicating the absence of nanoparticle aggregation [15]. Under these optimized conditions, the direct Cr(VI) signal was minimal and non-linear, while the calibration curve at 400 nm exhibited a slope of (-124 ± 1) x 10^{-4} μM^{-1} with a correlation coefficient of 0.990 ± 0.001 (Table 1), demonstrating enhanced sensitivity and stability.

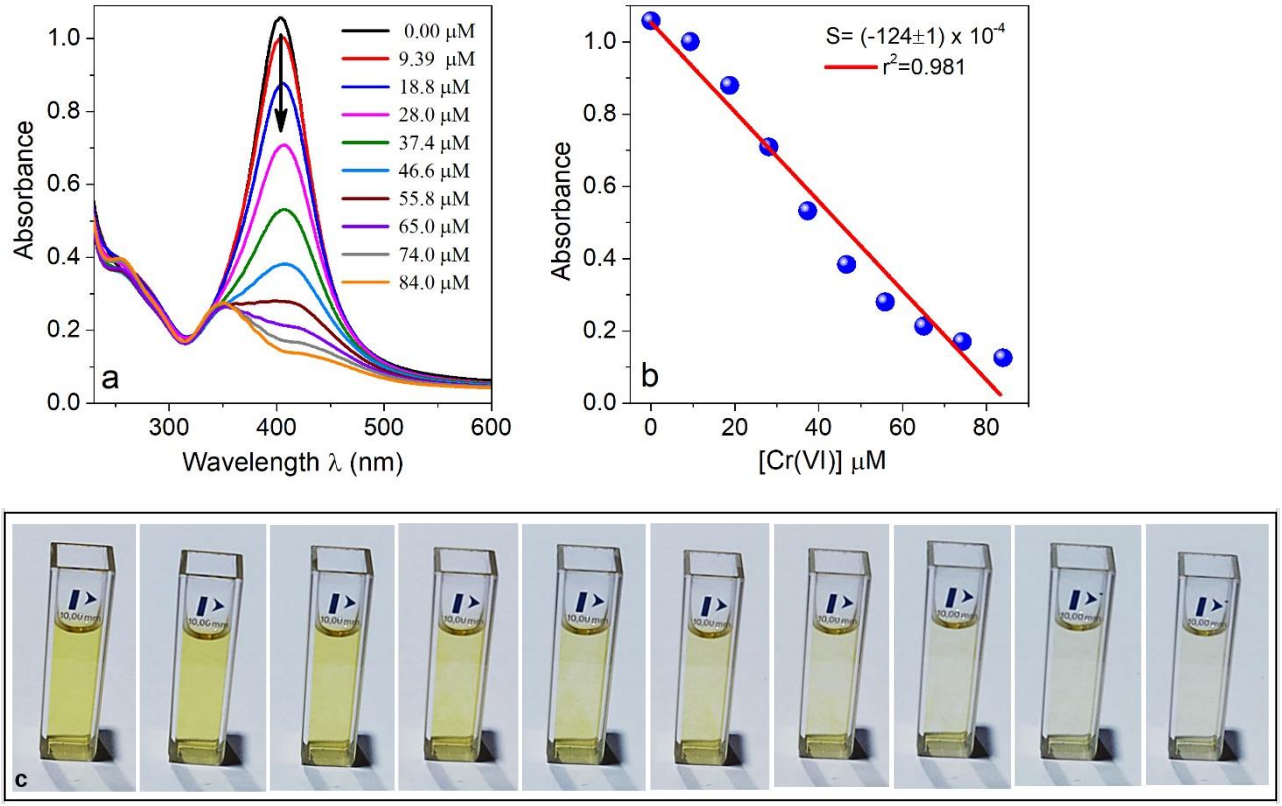

Figure 4. a) Response of AgNPs@starch at 400 nm upon addition of Cr(VI) in the range 0 to 84 µM. b) Calibration curve of Absorbance *vs* µM Cr(VI). c) Solution color change upon AgNPs@starch aliquots addition.

Table 1. Parameters of absorbance *vs* Cr(VI) concentration calibration curves at pH 4 from Figure 4, and Figure 5. Experiments were performed in DI water (free ions), in the presence of interferents as Cr(III), Ca^{2+}, Mg^{2+}, Br^-, Cl^-, and in real water samples such as natural mineral water (NMW-1), tap water and Suquía River water.

Sample	**$Cr_{(VI)}$ µM**	**Slope ($x10^{-4}$ μM^{-1})**	**r^2**	**λ (nm)**
DI water	0-84	-124 ± 1	0.981±0.001	403
Cr(III)	0-85	-124±6	0.987±0.001	405
Br^-,Cl^-,Na^+	0-85	-120±5	0.98±0.005	406
Ca^{2+},Mg^{2+},NO_3^-	0-85	-123±5	0.970±0.005	401/406
NMW-1	0-81	-120±5	0.992±0.001	400
Tap water	0-81	-120±8	0.979±0.001	405
Suquía River water	0-84	-127±1	0.95±0.001	405/406

Quantification limit (LOQ) and detection limit (LOD) of $Cr_{(VI)}$ with AgNPs

As mentioned in the Introduction, being hexavalent chromium a Group A human carcinogen, a guideline value (GV) of 50 $\mu g \cdot L^{-1}$ for total chromium is recommended by the WHO, based on the achievable removal by current treatment technologies, analytical measurability, and toxicological evidence. The health risk assessment for chromium in drinking water is derived from recent high-quality chronic toxicity and mode-of-action studies involving both Cr(III) and Cr(VI). Consequently, the current GV of 50 $\mu g \cdot L^{-1}$ (total chromium) is considered adequately protective of human health and has been retained in the most recent WHO guidelines (2020) [5].

The limits of detection (LOD = $3 \cdot S_r/m$) and quantification (LOQ = $10 \cdot S_r/m$) were determined according to standard analytical protocols, where S_r is the standard deviation of the regression and *m* is the slope of the calibration curve relating signal intensity to analyte concentration [35-37]. The LOD obtained in this study, (0.21 ± 0.02) µM, is below the threshold required for environmental monitoring of chromium in surface waters, as specified by WHO guidelines [5]. The corresponding LOQ was 0.69 µM (≈36 $\mu g \cdot L^{-1}$).

These results demonstrate a significant improvement over several previously reported methods for Cr(VI) detection. Compared with starch-stabilized AgNPs reported by others [14], which exhibited LODs of 0.93 µM (in the 0-6 µM range) and 11.57 µM (in the 9.79-80 µM range) at pH 3, our method achieves a much broader linear range (0-83 µM) while reducing the LOD by a factor of approximately 4.5. This enhanced dynamic range markedly improves the applicability of the method for practical environmental monitoring. A very low detection limit of 1 nM was reported by A. Ravindrana et al. [15], calculated from the ratio of absorbance at 550 nm to that at 390 nm. However, the absorption band around 550 nm is typically associated with silver nanoparticle aggregation. Since nanoparticle aggregation is highly sensitive to experimental conditions (e.g., ionic strength, pH, and colloidal stability), the reproducibility of this signal may vary across experiments. Therefore, although a 1 nM limit of detection was reported based on the A_{550}/A_{390} ratio, the robustness of such low detection limits warrants careful evaluation.

Although ascorbic acid-coated AgNPs have been reported to reach exceptionally low LODs of 0.05 µM at pH 7.6 [16], their sensitivity was limited to a very narrow working range (0.07-1.84 µM) and compromised by nanoparticle aggregation arising from redox interactions with Cr(VI) species, likely forming Cr(III) complexes. Similarly, biosynthesized AgNPs with working ranges of 0.19-1.92 mM [7], and polyethylenimine-stabilized Ag nanoclusters facilitating the chromogenic reaction between Cr(VI) and 3,3′,5,5′-tetramethylbenzidine (TMB) in the 5-100 µM range [17], exhibited LODs of 1.92 µM and 1.1 µM, respectively (both substantially higher than those obtained in this study).

Rosmarinic acid-capped AgNPs, in the presence of ascorbic acid and after a 10-minute incubation period [18], achieved the lowest reported minimum detectable concentration (0.04 µM); however, their linear range was restricted to 0-10 µM, with reliable performance only up to 1 µM. In contrast, the present AgNPs@starch-based system combines high sensitivity with a broad linear range, offering a balanced compromise between detection limit, stability, and operational simplicity. Table 2 summarizes these results.

Table 2. LOD values of AgNPs@starch in comparison with reports of the literature using silver nanoparticles for sensing Cr(VI).

Sensor Type / Reference	**Linear Range (µM)**	**LOD (µM)**	**Key Features**
AgNPs@starch (this work)	0-85	0.21	DI-water, pH 4. Buffer pH 4,75 using EDTA as stabilizer. High sensitivity, rapid analysis, below EPA limit for drinking water
AgNPs/starch [14]	0-6 9.79-80	0.93 11.57	pH 3 .EDTA as stabilizer -. Rapid analysis
AgNPs [15]	0.001-10	0.001	Absorbance ratio A(550 nm / 390 nm)
AgNPs/ascorbic acid [16]	0.07-1.84	0.05	pH 7.6 -Aggregation of AgNPs by Cr(III)
Biosynthesized AgNPs [7]	192-1920	1.92	Shift from 451 to 372 nm, and appearance of new peak at 261 nm with Cr(VI) addition
Rosmarinic acid-capped (Ro-AgNPs) [18]	0-10	0.04	Selective colorimetric detection; 6 min incubation

Overall, these comparisons highlight that while some systems can reach slightly lower absolute LODs, they often suffer from limited working ranges, long incubation times, or instability under operational conditions. The proposed method therefore represents a more versatile, rapid, and robust approach for Cr(VI) detection, with significant potential for environmental monitoring applications.

3.3. *Determination of Cr(VI) with AgNPs in presence of Cr(III), interferences and real water samples.*

Interference assays for Cr(VI) determination were performed under optimized conditions using 57 µM AgNPs@starch and 48 µM EDTA at pH 4. As previously reported [14], EDTA acts as a masking agent, effectively eliminating the interfering effects of heavy metal cations without impairing analyte response. Furthermore, EDTA has been shown to prevent the aggregation of silver nanoparticles induced by Cr(III) ─the reduction product of Cr(VI)─ by forming stable Cr(III)-EDTA complexes [16].

Figure 5a shows the absorbance spectra of AgNPs@starch with 48 µM EDTA, recorded at 400 nm upon the addition of increasing Cr(III) concentrations (9.6, 19, 28, and 38 µM). No significant change in absorbance was observed, confirming that Cr(III) does not interact with or affect the optical properties of AgNPs@starch under the experimental conditions.

Figure 5b displays the absorbance spectra of AgNPs@starch (57 µM) in the presence of 19 µM Cr(III) upon sequential addition of Cr(VI) at concentrations of 0, 9.6, 19, 28.6, 38, 47, 57, 66, 75, 85, and 94 µM. The slope (-124 ± 6) × 10^{-4} μM^{-1} and correlation coefficient (r^2 = 0.987 ± 0.001) are in close agreement with those obtained in deionized (DI) water (Figure 4b), indicating that Cr(III) does not interfere with Cr(VI) detection.

Figure 5c presents the absorbance spectra of AgNPs@starch upon Cr(VI) addition in the presence of 0.58 mM NaBr and 0.58 mM NaCl. The maximum absorbance was observed at 406 nm. Cr(VI) aliquots were added at concentrations of 0, 9.6, 19, 29, 38, 48, 57, 66.5, 76, and 85 µM. The slope (-120 ± 5) × 10^{-4} μM^{-1} closely matches that of the ion-free system, confirming that common halide ions exert negligible interference. The corresponding calibration data are summarized in Table 1.

Figure 5d shows the absorbance spectra of AgNPs@starch recorded at pH 4 in the presence of 4.45 mM $Ca(NO_3)_2$ (178 $mg \cdot L^{-1}$ Ca^{2+}) and 4.3 mM $Mg(NO_3)_2$ (103 $mg \cdot L^{-1}$ Mg^{2+}). Cr(VI) was sequentially added in concentrations of 5.5, 8.6, 17, 26, 34, 43, 51, 59.5, 68, 76, 85, 93, and 102 µM. A linear calibration range was established between 0 and 80 µM Cr(VI) (Figure 5g). The slope (–123 ± 5) × 10^{-4} μM^{-1} and correlation coefficient (r^2 = 0.970 ± 0.005) were comparable to those obtained in the absence of interfering species, even under elevated cation concentrations (Table 1). This demonstrates the robustness of the sensing system, as the Ca^{2+} and Mg^{2+} levels used were significantly higher than those typically present in drinking or natural mineral waters. Such stability under exaggerated interference conditions indicates that the AgNPs@starch sensor is suitable for real environmental samples. Future experiments will focus on evaluating performance at environmentally relevant ion concentrations to further validate field applicability.

Figure 5e displays the absorbance spectra of AgNPs@starch in natural mineral spring water with low mineralization (NMW-1), adjusted to pH 4. The composition of this Cr(III)-free sample, described in the *Experimental Section*, was used to simulate natural water conditions. Cr(VI) was added in the range of 0.9, 15, 18, 27, 36, 46, 54, 63, 72, 81, 90, 108, and 125 µM. The calibration curve constructed from 0 to approximately 85 µM Cr(VI) yielded a slope of (-120 ± 5) × 10^{-4} μM^{-1} and r^2 = 0.992 ± 0.001 (Table 1).

Figure 5f presents the absorbance spectra of AgNPs@starch in tap water at pH 4 following Cr(VI) addition in the range 0-125 µM (0, 9.15, 18, 27, 36, 45.5, 54, 63, 72, 81, 90, 99, 108, and 125 µM). The composition of the tap water sample is provided in the *Experimental Section*. The calibration curve, constructed between 0 and ~85 µM Cr(VI), exhibited a slope of (-120 ± 8) × 10^{-4} μM^{-1} and r^2 = 0.979 ± 0.001 (Table 1).

To evaluate the applicability of the AgNPs@starch sensing system in real environmental matrices, experiments were performed using contaminated river water collected from the Suquía River (Córdoba, Argentina). Prior to the addition of the nanoparticles, the filtered water sample was treated with H_2O_2 and EDTA and allowed to react for 5 min. This simple pre-treatment step was introduced to minimize potential matrix interferences. The concentrations of the additives were systematically optimized to 0.3 mM H_2O_2 and 48 µM EDTA to obtain a nanosensor performance comparable to that observed in ultrapure water.

Figure 5g shows the absorbance curves of AgNPs@starch in the contaminated Suquía River water at pH 4 under these conditions. After this treatment, the sensor response toward Cr(VI) was restored and became comparable to that observed in ultrapure water, as shown in Figures 5 g-h and summarized in Table 1. The calibration curve, constructed between 0 and ~84 µM Cr(VI) (0,9.5, 19, 28, 37.5, 47, 56, 65, 74.6, 84, 93, 102, 111) exhibited a slope of (-127 ± 1) × 10^{-4} μM^{-1} and r^2 = 0.95 ± 0.001.

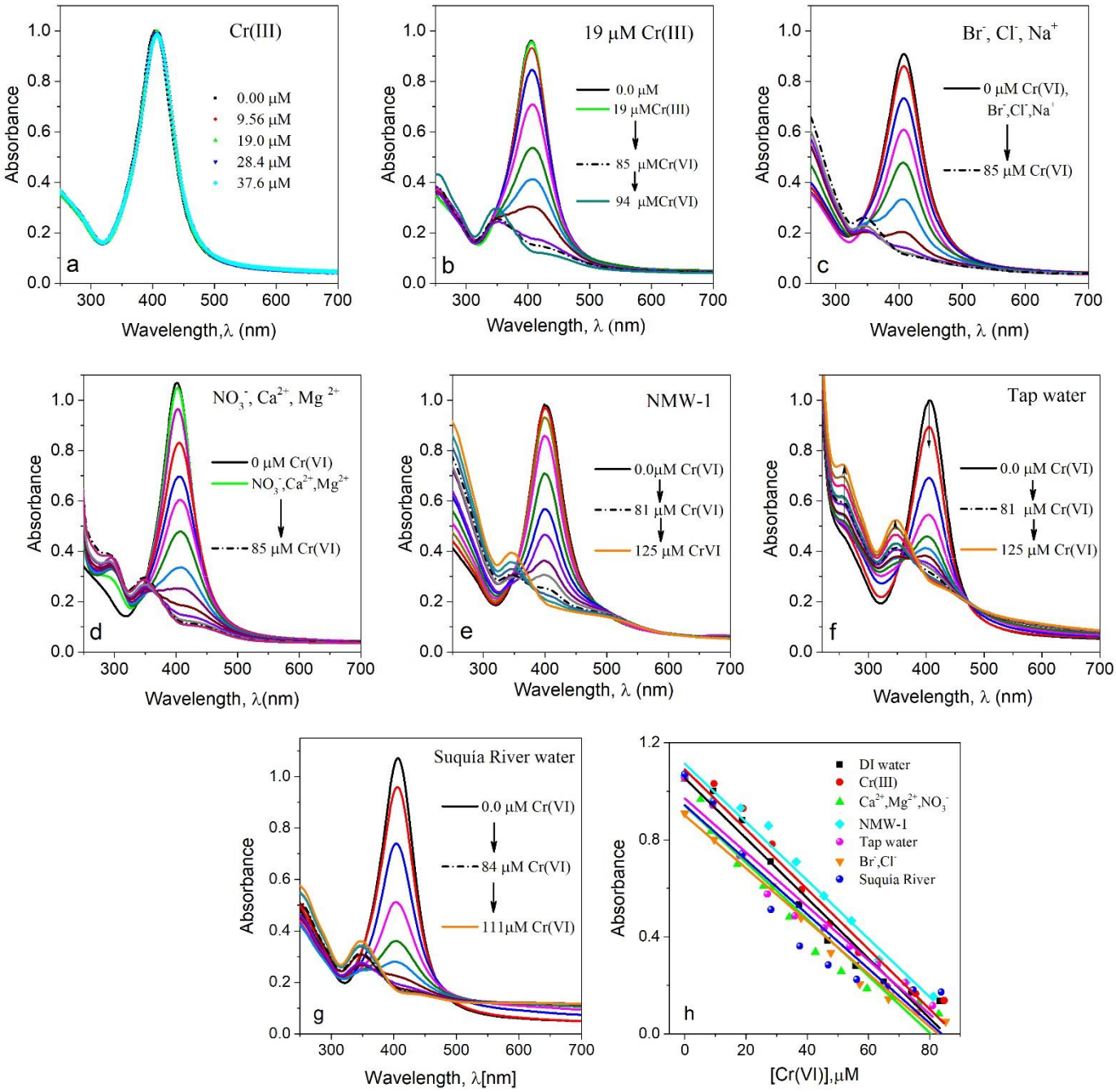

Figure 5. Absorbance spectra for 57 µM AgNPs@starch solution with 48 µM EDTA. a) Cr(III) in DI water. b)19 µM Cr(III) and Cr(VI) in DI water. c) 0.58 mM NaBr, 0.58mM NaCl and Cr(VI) in DI water. d) 4.4 mM $Ca(NO_3)_2$, 4.3 mM $Mg(NO_3)_2$ ions and Cr(VI) in DI water. e) Cr(VI) in mineral water (NMW-1). f) Cr(VI) in tap water. g) Cr(VI) in Suquía River water, h) Absorbance *vs* [Cr(VI)] (µM) for b), c), d), e), f) and g).

The lack of sensitivity of the AgNPs@starch sensor in non-pretreated contaminated river water, can be attributed to matrix effects caused by dissolved species naturally present in contaminated river water. Sulfide and related sulfur species present in contaminated river water may originate from sewage discharges, as from the municipal waste water treatment plant [38,39] where microbial sulfate reduction generates H_2S and other reduced sulfur compounds capable of passivating silver nanoparticle surfaces. Reduced sulfur species (e.g., HS^-/S^{2-}) and other reducing agents can interact strongly with silver surfaces, leading to partial passivation or surface modification of the AgNPs. The addition of H_2O_2 oxidizes these reduced species to more stable forms (e.g., sulfate), preventing their interaction with the nanoparticle surface. In parallel, EDTA acts as a chelating

agent for dissolved metal ions (such as Fe^{3+} or Cu^{2+}), which could otherwise adsorb on the nanoparticle surface or participate in competing reactions in the sensing system.
The relative error across all assays was ≤5%, determined by comparing the slope values of the calibration curves obtained in various matrices with that obtained for the DI water (ion-free) system (black line, Figure 5h). A summary of all calibration parameters and comparative results is presented in Table 1.

3.4. *Determination of Cr(VI) with AgNPs@starch in buffered solution of pH 4.75*

The sensitivity of AgNPs@starch toward Cr(VI) was further evaluated in a buffered medium (ABS, pH 4.75) composed of 0.2 M acetic acid/sodium acetate.

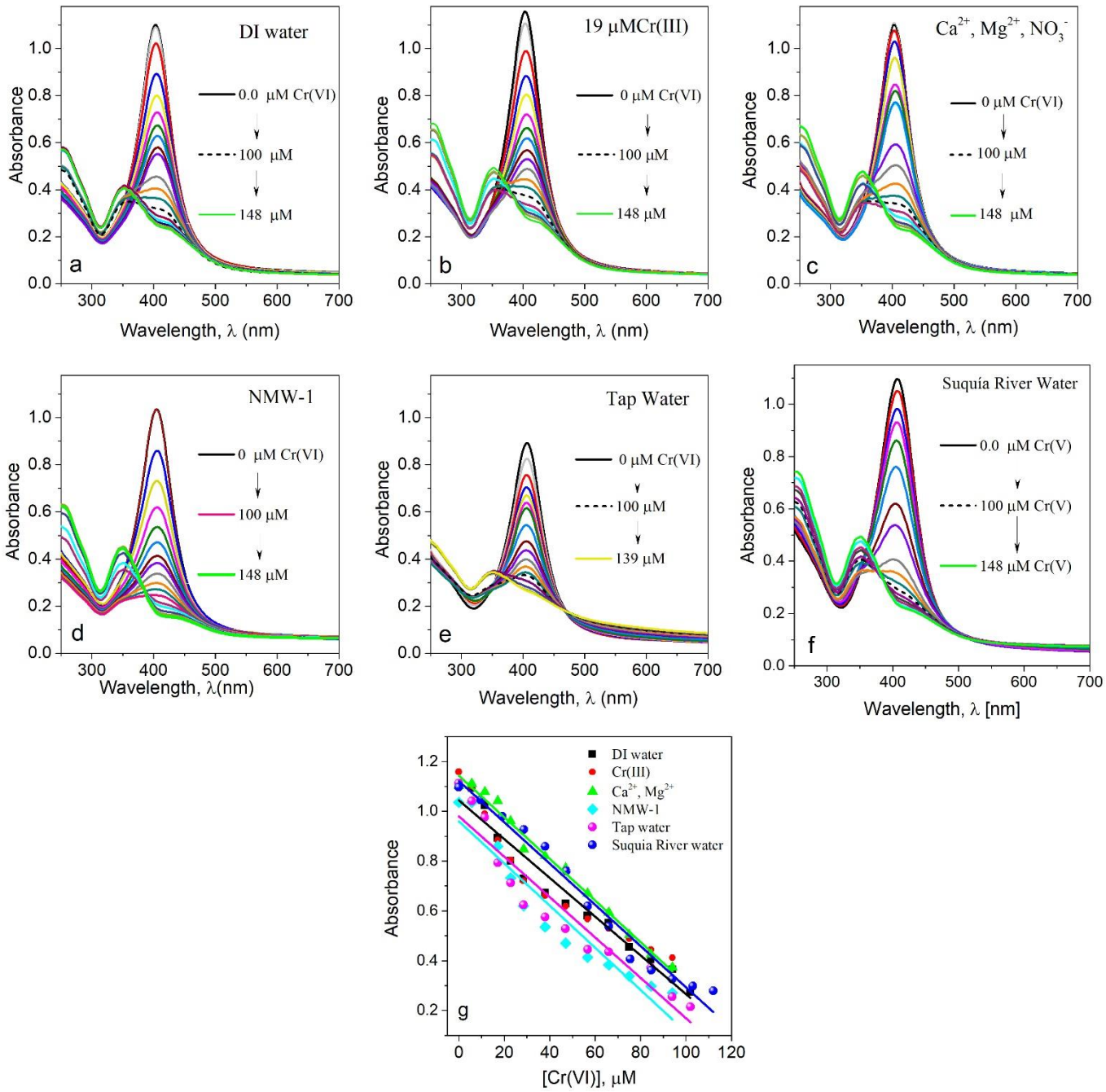

Figure 6. The absorbance spectra for 57 µM AgNPs@starch solution with 48 µM EDTA, in ABS of pH 4.75 upon the aliquots of Cr(VI) in: a) DI water. b)19 µM Cr(III) in DI water, c) 1.14 mM Ca^{2+}, Mg^{2+} and 2.28 mM NO_3 ions in DI water, d) mineral water (NMW-1), e) drinking water, f) Suquía River water. g) Absorbance *vs* [Cr(VI)] for a), b) , c), d), e) and f).

The use of a buffer was expected to enhance nanoparticle stability by mitigating oxidative degradation of AgNPs. As shown in Figure 6a, the decrease in absorbance intensity upon Cr(VI) addition in buffered DI water was slower than in the unbuffered medium, indicating improved nanoparticle stability. Cr(VI) was added in aliquots of 0, 5.7, 11, 17, 23, 28.5, 38, 47, 57, 66, 75, 84.6, 94, 103, 112, 121, 130, 139, and 148 µM. A linear calibration range was obtained from 0 to 100 µM Cr(VI), with a slope of (-83 ± 1) × 10^{-4} μM^{-1} and correlation coefficient $r^2 = 0.99 \pm 0.01$. The calculated detection limit (LOD) in ABS at pH 4.75 was 0.21 µM, closely matching that determined at pH 4 in DI water.

Assays performed in the buffered system (ABS, pH 4.75) with potential interferents and in real aqueous samples yielded results consistent with those obtained in the ion-free medium (Figure 6a).

The corresponding absorbance spectra for Cr(VI) addition are shown in Figures 6b to 6e. Figure 6b presents the response in the presence of 19 µM Cr(III) in ABS (pH 4.75, DI water), demonstrating negligible interference. Figure 6c displays the absorbance spectra for Cr(VI) in ABS (pH 4.75) containing 1.15 mM Ca^{2+} (46 $mg \cdot L^{-1}$), 1.15 mM Mg^{2+} (27.6 $mg \cdot L^{-1}$), and 2.3 mM NO_3^-, confirming that the presence of common ions did not significantly affect sensitivity or linearity.

Figures 6d and 6e show the absorbance curves obtained in buffered natural mineral water (NMW-1) and tap water, respectively. Figure 6f shows the absorbance curves obtained in buffered Suquía River contaminated water. Calibration parameters for all tested matrices are summarized in Table 3. The relative deviation in slope values compared to the reference system (ABS, pH 4.75, DI water) was ≤5%, indicating excellent reproducibility and robustness of the sensing platform under varying water chemistries.

It is worth noting that when the AgNPs@starch system was evaluated in the Suquía River water using an acetate/acetic acid buffer (pH 4.75-5) in the presence of 48 µM EDTA, the sensitivity toward Cr(VI) was comparable to that obtained in ultrapure water. Under these conditions, no additional H_2O_2 treatment was required. This behavior can be attributed to the mildly acidic medium, which likely suppresses the reactivity of reduced sulfur species and other potential interferents present in the river water. In addition, EDTA efficiently complexes dissolved metal ions that could otherwise interact with the nanoparticle surface. As a result, the AgNPs@starch system maintains its sensing performance toward Cr(VI) even in the complex river water matrix.

It is assumed that at comparable acidic conditions, the oxidation of AgNPs occurred more slowly in the buffered medium (pH 4.75) than in the unbuffered solution (pH 4). This behavior is attributed to the buffer's ability to maintain a stable pH, modulate the availability of oxidizing species (H^+ and dissolved O_2), and stabilize the local chemical environment around the nanoparticles. In unbuffered solutions, proton accumulation during $Ag^0 \rightarrow Ag^+$ conversion accelerates oxidation and nanoparticle dissolution, whereas in buffered systems (e.g., acetate), the generated protons are neutralized, preventing local acidification. Buffer anions may also coordinate Ag^+ ions, forming soluble Ag-buffer complexes that reduce the free Ag^+ activity and slow oxidation. Consequently, AgNPs@starch display greater chemical stability and resistance to oxidative degradation in buffered media than in unbuffered solutions of similar pH. Another significant advantage of using a buffered solution at pH 4.75 is that the nanoparticle-based sensing remained efficient even in contaminated river water. This indicates that the buffered medium helps mitigate matrix interferences, allowing reliable detection without altering the original sample composition through the addition of extra reagents such as hydrogen peroxide.

The overall comparison between buffered and unbuffered systems revealed that AgNPs@starch exhibited similar sensing efficiency under both conditions. Although the sensitivity achieved at pH 4 in unbuffered DI water was slightly higher, the buffered system (pH 4.75) allowed for an expanded Cr(VI) detection range while maintaining a comparable LOD. These findings confirm that the AgNPs@starch probe performs reliably across both buffered and unbuffered environments, supporting its applicability for practical water analysis.

Table 3. Parameters of absorbance vs Cr(VI) concentration curves using AgNPs@starch at ABS pH 4.75. Experiments were performed in DI water (free ions), in the presence of interferents as Cr(III), Ca^{2+}, Mg^{2+}, and in real water samples as natural mineral water (NMW-1), tap water and Suquía River water.

Samples	Cr(VI) (μM)	Slope (x 10^{-4} μM^{-1})	r^2	λ (nm)
ABS pH 4.75	0-100	83 ±1	0.99±0.001	402/406
Cr(III)	0-100	-82 ± 2	0.975±0.005	403/407
Ca^{2+},Mg^{2+},NO_3^-	0-100	-83 ± 3	0.988±0.001	403/405
NMW-1	0-100	-83± 3	0.970±0.008	404/406
Tap water	0-100	-81± 3	0.955±0.005	403/406
Suquía River water	0-100	-83±1	0.973±0.001	404/406

3.5 *Cyanide determination using AgNPs@starch as sensor*

The sensitivity of AgNPs@starch toward cyanide (CN^-) was evaluated by monitoring the absorbance changes of the surface plasmon resonance (SPR) band at approximately 400 nm. Figure 7a shows the SPR absorption band centered at 398 nm for a 71 μM AgNPs@starch solution in borate buffer (BBS, pH 8.4). The corresponding calibration curve, constructed from absorbance data in the range 0-85 μM CN^- (0, 9.5, 19, 29, 38, 48, 57, 66, 76, and 85 μM), is presented in Figure 7b. The linear regression yielded a slope of (74 ± 1) × 10^{-4} μM^{-1} with a correlation coefficient $r^2 = 0.99 \pm 0.01$, confirming the excellent analytical performance of AgNPs@starch as an anion sensor in an interference-free aqueous system.

The absorbance intensity decreased progressively with increasing cyanide concentration, accompanied by a visible color change of the colloidal suspension. This behavior can be attributed to oxidative dissolution of metallic silver by dissolved oxygen in the presence of CN^-. According to literature reports [2, 18], this process involves either the formation of soluble silver-cyanide complexes ($Ag^+ + 2CN^- \rightleftharpoons [Ag(CN)_2]^-$) or surface oxidation reactions that generate reactive oxygen species (ROS), leading to the formation of Ag_2O and AgCN. Both mechanisms contribute to the bleaching and spectral attenuation observed during cyanide addition.

We hypothesize that at low CN^- concentration, the predominant mechanism is surface-limited oxidation to $[Ag(CN)_2]^-$. At higher CN^- concentration, nanoparticles tend to aggregate rather than undergo complete dissolution. Such aggregation can reduce absorbance changes due to plasmon, which causes spectral shifts without necessarily resulting in a linear decrease in absorbance. At elevated CN^- levels, secondary processes (such as reactive oxygen species formation and partial precipitation of AgCN or Ag_2O) may occur. These processes lead to smaller incremental changes in absorbance per unit increase in cyanide concentration.

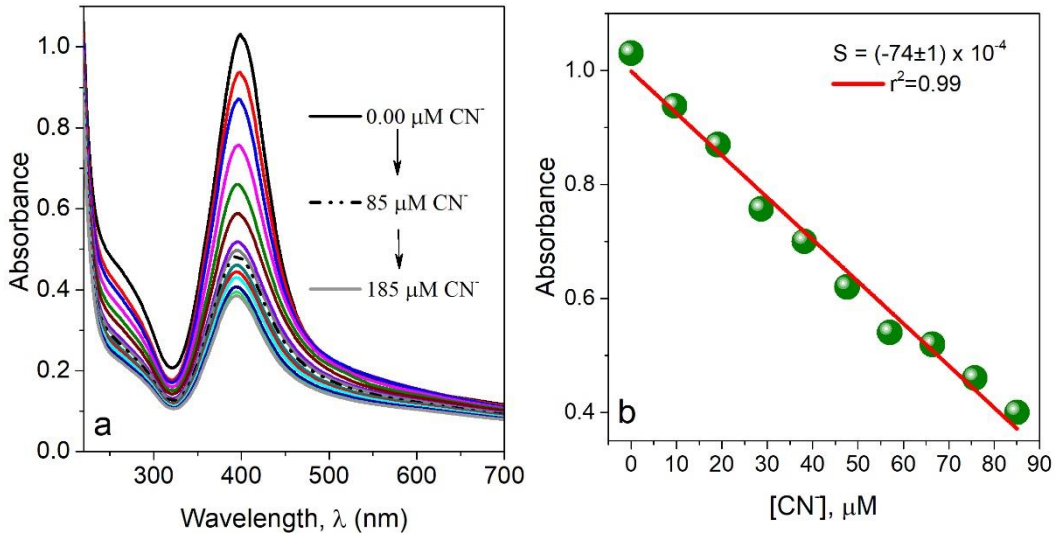

Figure 7. a) Response of AgNPs at 400 nm upon addition of CN^- for a range 0 to 85 μM in BBS pH 8.4. b) Absorbance *vs* CN^- μM , from 0 to 85 μM CN^-.

Quantification limit (LOQ) and detection limit (LOD) of cyanide with AgNPs@starch

The detection limit (LOD = 3 S_r/m) and quantification limit (LOQ = 10 S_r/m) for cyanide were determined in BBS (pH 8.4) following standard procedures [35-37]. The AgNPs@starch sensor exhibited a LOD of 0.24 µM and a LOQ of 0.81 µM, indicating high sensitivity and rapid response. The LOD obtained is well below the maximum contaminant level for cyanide in drinking water established by the U.S. EPA (0.2 $mg \cdot L^{-1} \approx 7.7$ µM) [3].

As summarized in Table 4, the analytical performance of AgNPs@starch compares favorably with previously reported AgNP-based cyanide sensors. While some biosynthesized or surface-functionalized AgNPs achieve slightly lower LODs, these typically require complex synthesis routes or long incubation periods. In contrast, the present system combines straightforward preparation, fast response, and robust performance, making it suitable for routine cyanide monitoring in aqueous samples.

Table 4. LOD values of AgNPs@starch in comparison with reports of the literature using silver nanoparticles for sensing cyanide.

Sensor Type / Reference	**Linear Range (µM)**	**LOD (µM)**	**Key Features**
AgNPs@starch (this work)	0-85	0.24	High sensitivity, rapid analysis, below EPA limit for drinking water
AgNPs -sodium dodecyl sulfate(SDS) [2]	16.7-133	0.18	AgNPs stabilized with SDS; Comparable LOD
Fluorescence assay (inner filter effect) [23]	0.5-600	0.25	Based on AgNPs absorption; comparable LOD
AgNPs -TritonX-100 (TX-100) [21]	500-3500	90	AgNPs stabilized with T X-100. Higher LOD than this work
Biosynthesized AgNPs (bitter orange bloom) [8]	0.05 -1.2	0.0079	Extremely high sensitivity and selectivity
AgNPs in agarose matrix [22]	1.5-120	0.69	Optical detection; higher LOD than this work
Rosmarinic acid-capped AgNPs (Ro-AgNPs) [18]	0-0.17	0.01	Selective colorimetric detection; 6 min incubation

3.6 *Determination of cyanide with AgNPs@starch in presence of interferences and real aqueous samples*

Figures 8a-8e illustrate the absorbance spectra obtained during cyanide determination in the presence of common ionic interferents and in real water matrices, all conducted in BBS (pH 8.4). Figures 8a and 8b show the spectral behavior of AgNPs@starch under controlled interference conditions, whereas Figures 8c to 8f correspond to natural and tap water samples.

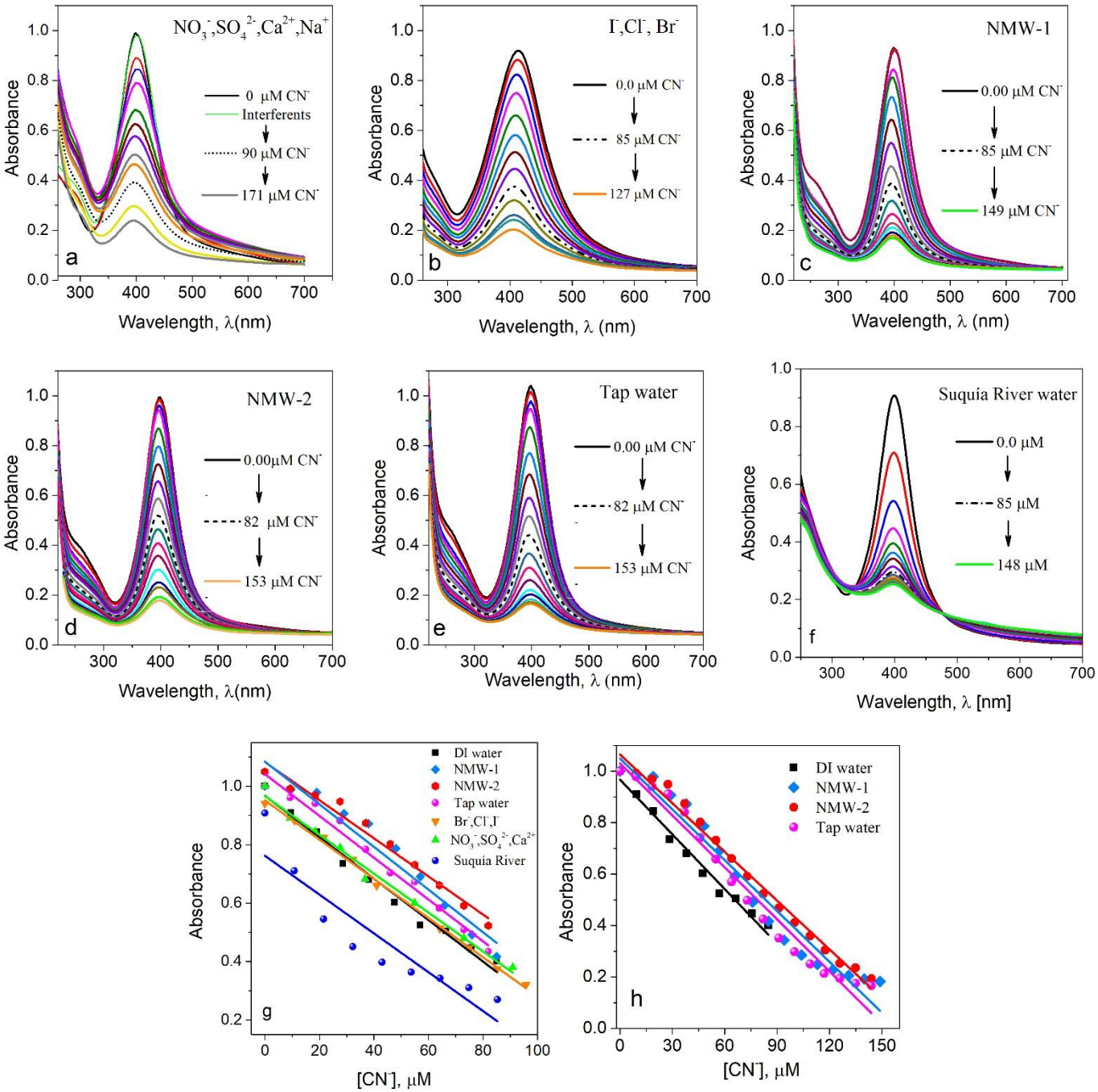

Figure 8. Absorbance spectra for 71 μM AgNPs@starch in buffer solution pH 8.4, upon the CN^- successive additions, using as interferents: a) NO_3^-, SO_4^{2-}, Ca^{2+} in DI water, b) Br^-, Cl^-, I^- in DI water, c) NMW-1, d) NMW-2, e) Tap water, f) Suquía River water. g) Absorbance *vs* CN^- (μM) for DI water and the experiments in a), b), c), d), e) and f). h) Calibration curves for tap water, NMW-1, NMW-2 between 0-150 μM CN^-.

Effect of cations and anions. Figure 8a presents the spectral evolution of AgNPs@starch upon CN^- addition in the presence of 2.3 mM $Ca(NO_3)_2$ (92 mg·L^{-1} Ca^{2+}) and 0.2 mM Na_2SO_4 in BBS (pH 8.4). CN^- was added in aliquots of 0, 9.2, 18.5, 27.6, 37, 55, 64, 73, 82, and 90 μM. The corresponding calibration parameters are summarized in Table 3. Figure 8b displays the spectra for AgNPs@starch in the presence of halide anions (0.58 mM NaCl, NaBr, and KI; equivalent to 20.6, 46.3, and 73.6 mg·L^{-1} of Cl^-, Br^-, and I^-, respectively). The CN^- concentrations ranged from 0 to 127 μM, with the calibration curve constructed for 0-85 μM. The aliquots of CN^- added were: 0, 10.8, 21.5, 32, 43, 54, 64, 75, 85, 106, 117, up to 127 μM. The resulting slope closely matched that of the deionized-water system, confirming that halides do not significantly interfere with CN^- detection.

Performance in real water samples. Figure 8c shows the absorbance spectra for AgNPs@starch in natural mineral water 1 (NMW-1) at pH 8.4, with CN^- additions from 0 to 149 µM. Figures 8d and 8e display analogous spectra for natural mineral water 2 (NMW-2) and tap water, respectively, under the same pH conditions and CN^- addition series up to 153 µM. The consecutive aliquots of CN^- were: 0, 9.2, 18, 27, 37, 46, 55, 64, 73, 82, 91, 100, 109, 117, 126,135, 144, up to153 µM. Figure 8f presents the spectral curves for AgNPs@starch in the water sample from Suquía River. The river sample was buffered at pH 8.4 and 150 µM EDTA together with 0.3 mM H_2O_2 were added. The consecutive aliquots of CN^- were: 0, 10, 21, 32, 43, 53, 64, 75, 85, 96, 106, 116, 127, 137 and 148 µM. The calibration curve was built between 0-85 µM CN^-. The calibration plots (absorbance vs. $[CN^-]$) corresponding to all systems (Figures 8a to 8f) are compiled in Figure 8g, and the regression parameters are listed in Table 5.

In alkaline medium (pH 8.4), cyanide strongly coordinates silver and induces oxidative dissolution of surface Ag^0 atoms from the AgNPs, forming the soluble complex $[Ag(CN)_2]^-$. This ligand-induced etching decreases the plasmonic absorbance of the nanoparticles. The addition of EDTA masks interfering metal ions present in Suquía River water, preventing competing complexation reactions and preserving the sensor response toward cyanide. Hydrogen peroxide can oxidize sulfide species (HS^-/S^{2-}) commonly present in natural waters into oxidized sulfur species such as sulfate. This reaction occurs under both acidic and alkaline conditions, although the kinetics depend on pH. In the present alkaline system (pH 8.4), H_2O_2 helps removing sulfide species that could otherwise form Ag_2S on the nanoparticle surface and interfere with cyanide detection. Hydrogen peroxide can also promote the oxidative dissolution of surface Ag^0 atoms into Ag^+, which are rapidly complexed by cyanide to form the highly stable $[Ag(CN)_2]^-$ soluble complex. This coupled oxidation-complexation process accelerates the etching of AgNPs, leading to a pronounced decrease in the plasmonic absorbance. Meanwhile, EDTA acts as a masking agent for metal ions present in Suquía River water, suppressing potential interferences such as competitive complexation, redox catalysis, or nanoparticle aggregation. The combined effect of Ag oxidation, cyanide complexation, and metal-ion masking enhances the sensitivity of the AgNPs-based sensor toward cyanide detection.

Table 5. Parameters of absorbance vs $[CN^-]$ concentration curves using AgNPs@starch at BBS pH 8.4. Experiments were performed in DI water (free ions), in the presence of interferents as Ca^{2+}, Na^+, NO_3^-, SO_4^{2-}, Br^-, Cl^-, I^- and in real water samples as natural mineral water (NMW-1, NMW-2), tap water and Suquía River water.

Samples BBS pH 8.4	**CN^- (µM)**	**Slope (x 10^{-4} µM)$^{-1}$**	**r^2**	**λ (nm)**
DI water	0-85	-74± 3	0.994±0.001	400
NMW-1	0-85	-73± 3	0.974±0.001	395/399
NMW-2	0-85	-65± 2	0.989±0.001	395/398
Tap water	0-85	-71± 3	0.991±0.001	395/399
NO_3^-,SO_4^{2-}	0-90	-67± 2	0.994±0.005	400/398
Br^-,Cl^-,I^-,	0-90	-66± 2	0.995±0.001	414/406
NMW-1	0-140	-66 ± 3	0.989±0.001	395/399
NMW-2	0-140	-63± 2	0.994±0.001	395/398
Tap water	0-140	-67± 3	0.987±0.001	395/399
Suquía River water	0-85	-66±2	0.92±0.001	400

Fluoride and chloride are the most common anionic interferents in potable waters. The fluoride concentrations in the tested samples were low (1.2 mg·L^{-1} in NMW-1, < 0.6 mg·L^{-1} in NMW-2, and 0.22 mg·L^{-1} in tap water) suggesting negligible interference with cyanide detection. Tap water contained total and free chlorine concentrations of 1.3 mg·L^{-1} and 1.1 mg·L^{-1}, respectively, and a chloride concentration of 14.5 mg·L^{-1}. The calibration curves for DI water, mineral waters, and tap water, all prepared in BBS (pH 8.4), are compared in Figure 8h. Across all systems, the linear range for CN^- detection extended from 0 to 150 µM, and the relative deviation in slope values with respect to the DI water reference was ≤ 5%.

In general, the decreased slope observed when extending the cyanide concentration range indicates a reduction in the effective sensitivity at higher concentrations. This behavior is likely attributable to partial saturation of the AgNPs oxidation process, where additional cyanide produces smaller absorbance changes, and/or the onset

of secondary processes such as nanoparticle aggregation or surface precipitation of AgCN and Ag_2O. The change in the calibration curve slope may reflect a transition in the AgNPs oxidation mechanism, shifting from a primarily surface-limited reaction at low cyanide concentrations to a diffusion-controlled or aggregation-influenced process at higher concentrations.

These results demonstrate that AgNPs@starch provides selective and stable detection of CN^- even in the presence of common cations and anions typically found in natural and drinking waters, confirming its applicability for real environmental monitoring.

4. Conclusion

AgNPs@starch solutions function as selective colorimetric sensors for the determination of chromium(VI) and cyanide anions in aqueous media. The single SPR band at 400 nm confirms the uniform morphology of the synthesized nanoparticles, while distinct absorbance variations in the presence of target analytes reveal their high responsiveness.

For Cr(VI) detection, optimized conditions at pH 4 with EDTA minimized background coloration effects, achieving a detection limit of 0.2 μM. Measurements in acetate buffer (ABS, pH 4.75) extended the linear range while maintaining similar sensitivity. A key advantage of the pH 4.75 buffered solution is that nanoparticle-based sensing remained effective even in contaminated river water. This suggests the buffer mitigated matrix interferences, enabling reliable detection without additives. The acetate buffer at pH 4.75 controlled the chemical speciation of sulfide species and stabilized the nanoparticle surface, thereby preserving AgNP reactivity and restoring sensing performance.

For cyanide, optimized detection in borate buffer (BBS, pH 8.4) yielded a LOD of 0.24 μM. Interference studies and analyses of real water samples (including natural mineral and tap waters) confirmed that AgNPs@starch retains selectivity and accuracy, with calibration slopes differing by less than 5% from those obtained in DI water.

Cyanide detection at pH 8.4 using AgNPs@starch in contaminated river water was achieved following sample pretreatment with H_2O_2 as an oxidant and EDTA as a metal-ion complexing agent. The sensitivity obtained was comparable to that observed for the others water matrices evaluated.

Overall, the AgNPs@starch system demonstrates rapid response, high reproducibility, and versatility across different matrices, making it a robust and practical platform for environmental monitoring of toxic anions such as Cr(VI) and CN^-.

Acknowledgements

This work was partly funded by projects from CONICET, SeCyT-UNC and FONCyT (PICT-2020-0984). The authors thank LAMARX (FAMAF-UNC) for granting access to their facilities.

Supplementary Information

S1. Materials

The reagents and materials employed throughout this work are listed below:

Reagents for AgNPs synthesis:

Potassium chromate (K_2CrO_4, p.a., ACS, Cicarelli), potassium cyanide (KCN, p.a., Cicarelli), silver nitrate ($AgNO_3$, p.a., ACS), soluble starch (p.a., ACS, Cicarelli), and sodium borohydride ($NaBH_4$, Tetrahedron).

Buffer solutions:

- Borate buffer solution (BBS, pH 8.4): Sodium tetraborate ($Na_2B_4O_7$, p.a. 100%, Merck), boric acid (H_3BO_3, 100%, RA, ACS, Anedra), and sodium chloride (NaCl, 100%, J.T. Baker, ACS).
- Acetate buffer solution (ABS, pH 4.75): Sodium acetate (p.a., ACS, Cicarelli) and glacial acetic acid (p.a. 99%, ACS).

Reagents for selectivity and interference tests:

Ethylenediaminetetraacetic acid (EDTA, p.a. 99.4%, ACS, Cicarelli); sodium chloride (NaCl, 100%, J.T. Baker); sodium bromide (NaBr, p.a. 99%, Anedra); potassium iodide (KI, 99%, ACS, Sigma-Aldrich); calcium nitrate ($Ca(NO_3)_2$, p.a. 99%, Tetrahedron); magnesium nitrate ($Mg(NO_3)_2$, p.a., Tetrahedron); chromium(III) sulfate ($Cr_2(SO_4)_3 \cdot xH_2O$, x = 10–18, Tetrahedron); and sodium sulfate (Na_2SO_4, 99%, Merck).

Water Samples

- Natural Mineral Water 1 (NMW-1): Spring water of weak mineralization from the Andes mountain range. Composition (mg/L): Ca 30, Mg 3, Na 10, K 4, HCO_3^- 79, F^- 1.2.
- Natural Mineral Water 2 (NMW-2): Spring water from a protected reserve. Composition (mg/L): Ca 15, Mg 9, Na 55, HCO_3^- 145, $F^- < 0.6$.

Both NMW-1 and NMW-2 are commercial waters for human consumption.

- Tap Water: Collected from the southern water provision plant of Córdoba City (Argentina). Composition (mg/L): Ca 10.7, Mg 2.1, K 1.8, Na 7.3, Cl^- 14.5, total Cl 1.3, free Cl 1.2, F^- 0.22 (total F 0.26), $NO_3^- < 5$, $NO_2^- < 0.02$, Al 0.17, Fe < 0.05, Mn < 0.03. Total alkalinity: 27 mg/L.
- Suquía River water: Several studies have confirmed that the Suquía River in Córdoba (Argentina), particularly in the urban area of Córdoba city, is affected by significant anthropogenic contamination (see Table S1). The water sample was taken from the eastern edge of the city, under Bicentenario Bridge, where the composition of water is erratic and variable, because the industrial and domestic activities affect the water quality index. Monitoring studies have reported high ecological risk associated with pesticides, pharmaceuticals and other contaminants, with the highest levels detected downstream from the municipal wastewater treatment plant (Bertrand et al., *Science of The Total Environment,* 878 (2023), 163029.). Additional analyses indicate that land-use changes and urban activities strongly influence water quality in the basin (Paná et al., *Scientific Reports* 14 (2024) 4670), while environmental reports also highlight the presence of multiple urban pollution sources affecting the river system. Recently (S. Ruiz et al. *Frontiers in Microbiology,* 16 (2025) 1669531.) showed that **urban drainage and sewer infrastructure can contribute to environmental dissemination of antimicrobial resistance,** especially in rivers receiving urban runoff. Table S1 provides scientific evidence of pollution in the Suquía River.

Table S1. Main studies reporting contaminants in the Suquía River Basin (Córdoba, Argentina) from 2000 to 2025

Contaminant Category	Specific Examples / Groups	Notes	Reference
Pesticides & Organic Micropollutants	Atrazine (433.9 ng/L), Alpha-Cypermethrin (121.7 ng /L) Endosulfan sulfate (106.7 ng /L). In urban areas, the prevalent pesticide was alpha-cypermethrin.	Multiple pesticides and micropollutants in water and sediments	R. Bonansea et al., *Chemosphere* 90 (2013) 1860-1869. https://doi.org/10.1016/j.chemosphere.2012.10.007
Nutrients dynamic	Nitrates, Ammonium, total Phosphorus, etc	Urban expansion, agricultural activities	A. Pasquini et al., *Environ. Earth Sci.* (2012) 65, 453-467. https://doi.org/10.1007/s12665-011-0978-z
Nutrients, organic matter, turbidity, coliforms, oil grease, Surfactants (anionic as MBAS)	Nitrates, Ammonium, total Phosphorus, oil grease, domestic surfactants measured by MBAS method	Increasing nutrient loads and organic pollution downstream of the city.	S. Pesce et al., *Water Research.* 34, No. 11, (2000) 2915-2926 https://doi.org/10.1016/S0043-1354(00)00036-1
Pesticides & Pharmaceuticals (PPCPs) and cianotoxins	**Pesticides** Glyphosate, AMPA, Atrazine, Metolachlor, Chlorpyrifos) **Pharmaceuticals** Carbamazepine, Diclofenac, Ibuprofen, Naproxen, Paracetamol, Sulfamethoxazole, Trimethoprim.	Agriculture and Urban wastewater High ecological risk in both water and sediments	Bertrand et al., *Science of The Total Environment,* 878 (2023), 163029. https://doi.org/10.1016/j.scitotenv.2023.163029
Antibiotic-resistant bacteria	ESBL-, carbapenemase-producing enterobacterales	Present in urban stretch; linked to sewage overflows	S. Ruiz et al., *Frontiers in Microbiology*, 16 (2025) 1669531. https://doi.org/10.3389/fmicb.2025.1669531
Hormones & Viruses	Human-derived hormones, viral contamination	Indicates sewage influence	
Microplastics (presence)	Fibers and fragments reported	No recent published quantification	M. Kittner et al., *Journal of Hazardous Materials Advances* 8 (2022) 100185. https://doi.org/10.1016/j.hazadv.2022.100185
Water quality Index (WQI)	The lowest WQI is found in Córdoba city	WQI is negatively affected by agricultural and urban activities, while natural classes impacted positively	Paná et al., *Scientific Reports* 14 (2024) 4670 https://doi.org/10.1038/s41598-024-53604-0

Contaminant Category	Specific Examples / Groups	Notes	Reference
Heavy Metals	Zn, Cu and Pb are found downstream in river sediments	Untreated sewage in Córdoba city. The impact of sewage point source pollution	M. Monferrán et al., *Journal of Environmental Monitoring* 13 (2011) 398-409. https://doi.org/10.1039/c0em00545b
Heavy metals	Various metals in water/sediment	Part of broader pollution profile	L. Sepúlveda et al., *Revista Mexicana de Ciencias Geologicas* , 36 (2) (2019) https://doi.org/10.22201/cgeo.20072902e.2019.2.1037
Coliform bacteria	Fecal coliforms, *E. coli*	Exceeds some water quality thresholds	C. Merlo et al., *Ecología Austral* 27 (2017) 072-084. https://doi.org/10.25260/EA.17.27.1.0.401

The water from the Suquía River, upon reaching the power plant and prior to entering the water treatment plant, undergoes mechanical cleaning via screens of varying sizes. This process removes larger debris, such as leaves, branches, and other solids. Table S2 provides the composition of Suquía River water at the power plant for December 2025 and January 2026. This information was supplied by INA-CIRSA (Instituto Nacional del Agua - Centro de la Región Semiárida), Córdoba, Argentina.

Table S2. Composition of Suquía River water just before entering the water treatment plant.

Variable	Determination	Jan. 2026	Dec. 2025
pH (UpH)	pH measured in Lab.	7.4	7.6
Cond. Lab. (µS/cm)	Conductivity measured in lab.	165	254
Turb. Lab (UNT)	Turbidity measured in lab.	6.5	3.8
$N\text{-}NH_4^+$ (µg/l)	Nitrogen from Ammonium	85	54
$N\text{-}NO_3^-$ (mg/l)	Nitrogen from Nitrate	0.2	0.8
$N\text{-}NO_2^-$ (µg/l)	Nitrógeno de Nitrito	9	24
NT (mg/l)	Total Nitrogen	0.65	1.4
TSP (µg/l)	Total solublePhosphorus	61	101
SRP (µg/l)	Soluble reactive Phosphorus	33	49
TPH (µg/l)	Total Phosphorus	100	135
Alcalinity (mg/l)	Alcalinity	58	85
Hardness (mg/l)	Hardness	44	75
Ca (mg/l)	Calcium	13.6	23.3
Mg (mg/l)	Magnesium	2.4	4.2
Na (mg/l)	Sodium	12.8	25.2
K (mg/l)	Potassium	2	3
SO_4 (mg/l)	Sulphate	14	25.1
Cl (mg/l)	Chloride	5	8
F (mg/l)	Fluoride	0.59	0.87
Fe Sol (mg/l)	Soluble Iron	≤0.05	≤0.05
FeT (mg/l)	Total Iron	0.14	0.05
MnSol (mg/l)	Soluble Manganese	0.03	0.03
MnT (mg/l)	Total Manganese	0.05	0.03
TOC (mg/l)	Total Organic Carbon	7	6.1

Preparation of Standard Solutions

a) Cr(VI) determination:

A 5 mM Cr(VI) aqueous stock solution (K_2CrO_4/H_2SO_4) was prepared, adjusting the pH to 4 with H_2SO_4 solution. From 1.85 mM AgNPs@starch suspension an aliquot of 57 µM is taken and it is added into the quartz cell together with 48 µM EDTA, and adjusted to the desired pH (2 or ≥ 4).

For buffered conditions, ABS (pH 4.75) was prepared from 0.1 M acetic acid and 0.1 M sodium acetate.

Suquía River water collected from an urban area was first filtered through a 0.22 µm membrane. A 1 mM H_2O_2 stock solution was prepared using the filtered river water as the solvent. Different concentrations of H_2O_2 were then evaluated directly in the river water matrix. The system was finally optimized at 0.3 mM H_2O_2, 48 µM EDTA, and 57 µM AgNPs, with the pH adjusted to 4.

b) Cyanide determination:

A 5 mM KCN stock solution (pH 9) was prepared in deionized water. The borate buffer (BBS, pH 8.4) was prepared from 0.1 M H_3BO_3, 0.075 M NaCl, and 0.025 M $Na_2B_4O_7$. A 50 mM EDTA pattern solution of pH 8 was prepared.

Measurements were conducted by adding aliquots of the standard solution into a quartz cell containing 71 µM AgNPs dispersed in BBS (pH 8.4).

The measurements using filtered Suquía River water were optimized at 0.3 mM H_2O_2, 150 µM EDTA, and 71 µM AgNPs dispersed in BBs (pH 8.4).

S2. Direct Determination of Chromium

The direct detection of Cr(VI) based on the intrinsic color of the chromate ion was evaluated by UV–Vis spectrophotometry at 348 nm and 257 nm. Spectra for 48 µM EDTA solutions in (a) deionized (DI) water, (b) natural mineral water (NMW-2), (c) tap water (Córdoba City) and (d) Suquía River water, adjusted at pH 4 are shown in Figure S1 (a-d).

Water samples were adjusted to pH 4 and spiked with Cr(VI) aliquots ranging from 0 to 190 µM (0, 10, 20, 29.5, 39, 49, 59, 68, 78, 87.5, 97, 106, 116, 125, 135, 153, 172, 190 µM). Calibration curves (insets in Figure S1 a-c) display slope values comparable to those obtained at 348 nm and 256 nm in Figure 3b. Suquía River water was adjusted from 0 to 170 µM (0,9.8, 19, 29, 39, 48.5, 58, 68, 77, 87, 96, 106, 115, 115, 124, 134, 143, 152, 161, 170), as shown in Figure S1 d.

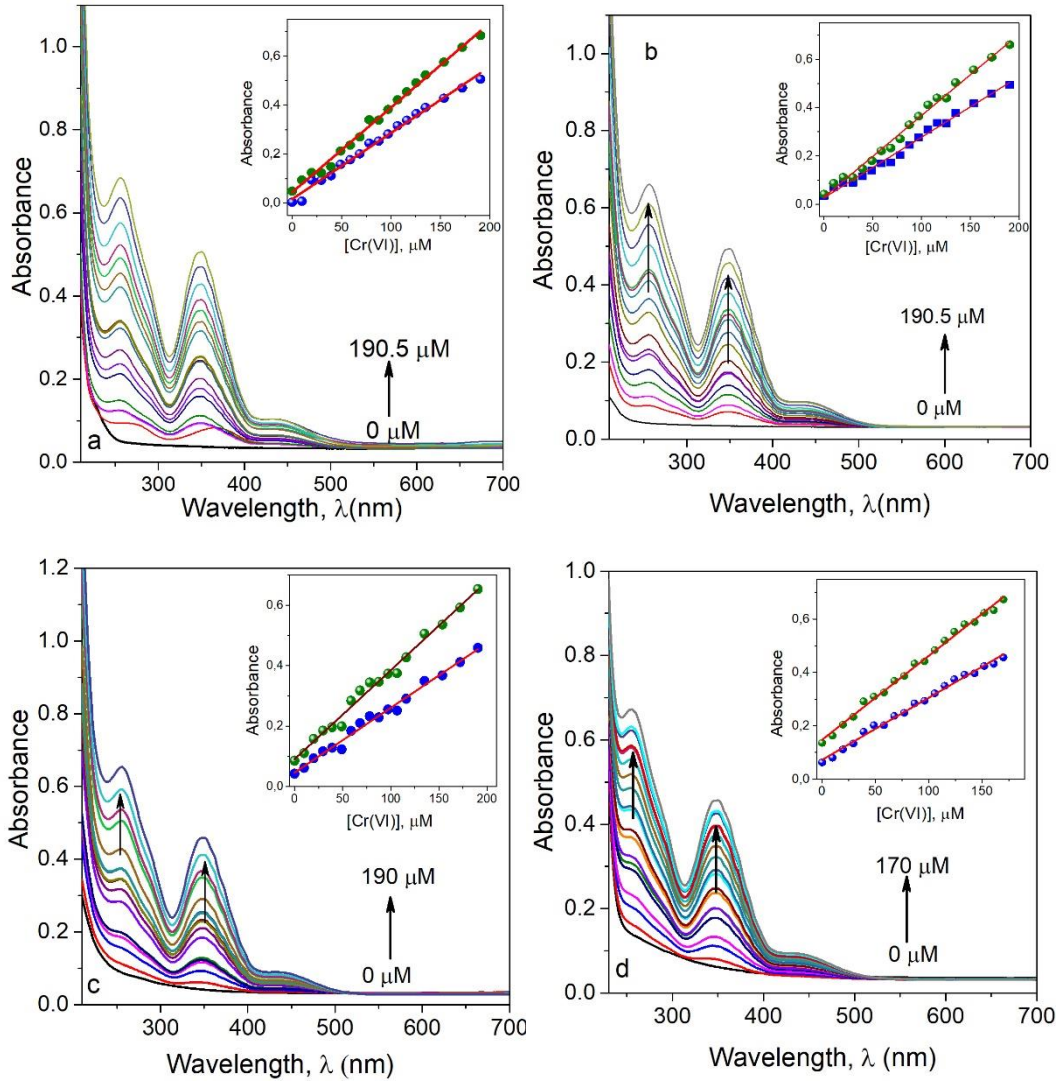

Figure S1. Spectra of direct Cr(VI) determinations using 45 µM EDTA at pH 4 as stabilizer. a) DI water. b) Natural mineral water (NMW-2). c) Tap water. d) Suquía River water.

The results are summarized in Table S3, which includes both the direct Cr(VI) measurements and those derived from Figure 3b (at pH 4).

While direct quantification of Cr(VI) up to 190 µM was feasible, sensitivity decreased substantially at lower concentrations, where the AgNPs-based sensor exhibited optimal performance.

Table S3. Parameters of absorbance vs Cr(VI) concentration curves measured without AgNPs@starch, at pH 4. Experiments were performed by direct coloration of Cr(VI) at 256 nm and 348 nm in DI and real aqueous samples.

Aqueous medium	**Cr(VI)**	**Direct Cr(VI)**	
		λ=348 nm	**λ=256 nm**
	μM	**Slope (x 10^{-4} μM^{-1})**	**Slope (x 10^{-4} μM^{-1})**
DI water pH 4(From Fig 3b)	70-220	27±3 r^2=0.990±0.003	36±3 r^2=0.990±0.003
DI water pH4	0-190	27±3 r^2=0.990±0.001	35+1 r^2=0.990±0.001
NMW-1 pH4	0-190	25±1 r^2=0.990±0.001	34±1 r^2=0.990±0.001
Tap water pH4	0-190	22±3 r^2=0.990±0.005	30±3 r^2=0.990±0.005
Suquía River water	0-170	23±1	32±3

S3. Effect of EDTA as stabilizing agent in Cr(VI) detection

The purpose of including of EDTA in Cr(VI) determination at pH 4 - 4.75 is to suppress interference effects. At pH 4-5, EDTA acts as an effective masking agent by forming stable complexes with potentially interfering heavy metal cations without significantly affecting the electrochemical response of Cr(VI). Moreover, EDTA prevents AgNPs aggregation induced by Cr(III) through the formation of stable Cr(III)-EDTA complexes, thereby enhancing colloidal stability.

The general redox reaction (without EDTA) is:

$HCrO_4^- + 3Ag_{(s)} + 7H^+ \Leftrightarrow Cr^{3+} + 3Ag^+ + 4H_2O$

So, if there is no EDTA in the solution, Cr(VI) reduces to Cr(III) and Ag(0) oxidizes to Ag(+). In this case, Cr(III) can bridge negatively charged AgNPs surfaces thereby forming AgNP aggregates.

On the other hand, if there is EDTA acting as stabilizer in the solution, the following reactions occur:

$HCrO_4^- + 3Ag_{(s)} + 7H^+ \Leftrightarrow Cr^{3+} + 3Ag^+ + 4H_2O$
$Cr^{3+} + EDTA \rightarrow [Cr(EDTA)]^-$

EDTA complexes Cr(III), preventing nanoparticle cross-linking. Therefore, EDTA can indeed prevent Cr(III)-induced aggregation. This is consistent with colloidal chemistry principles.

We propose a localized and dynamic reorganization of the polymer shell occurring at the nanoparticle/solution interface during the redox process. We suggest that the oxidation of surface Ag^0 atoms induces localized changes in the interfacial coordination environment.

The starch layer stabilizing the AgNPs is primarily maintained through hydrogen bonding and weak interactions with silver involving hydroxyl groups of amylose chains. These interactions are dynamic and non-covalent in nature. Upon exposure to Cr(VI), the oxidation of surface Ag^0 to Ag^+ modifies the surface charge density and coordination state, which can promote a localized and reversible reorientation of hydroxyl groups and conformational adjustment of nearby polymer segments.

Importantly, such interfacial rearrangement does not require cleavage or oxidation of the starch backbone. Rather, the polymeric chains behave as a soft and permeable layer capable of accommodating changes in surface chemistry while maintaining nanoparticle stabilization. This interpretation is consistent with the known dynamic behavior of polysaccharide-stabilized metal nanoparticles in aqueous media.

We propose that the reduction of hexavalent chromium Cr(VI) at mildly acidic pH occurs primarily through direct electron transfer at the nanoparticle/solution interface of starch-stabilized silver nanoparticles. Cr(VI) species such as $HCrO_4^-$ or $Cr_2O_7^{2-}$ approach the nanoparticle surface and accept electrons from surface-coordinated silver atoms (Ag^0), resulting in the oxidation of Ag^0 to Ag^+ and concurrent reduction of Cr(VI) to Cr(III). This interfacial electron transfer is consistent with the progressive loss of the characteristic surface plasmon resonance (SPR) band of AgNPs and the detected increase in Ag^+ concentration during reaction.

Although the starch capping layer adsorbed on the AgNP surface provides colloidal stability and steric protection, it does not form an impenetrable barrier to reactive species. Instead, localized partial displacement or reorganization of the starch shell occurs at the point of contact between Cr(VI) and the AgNP surface, enabling access of the oxidizing species to the metal surface. The dynamic nature of the capping layer allows regions of the silver surface to become transiently exposed, facilitating electron transfer. Following reduction, Cr(III) ions are rapidly sequestered by ethylenediaminetetraacetic acid (EDTA) in solution to form a highly stable $[Cr(EDTA)]^-$ complex, which drives the equilibrium toward further Cr(VI) reduction and prevents precipitation as chromium hydroxides under the experimental pH conditions. This oxidation alters the surface coordination environment and local charge distribution. Such changes are expected to weaken polymer-metal interactions in specific regions of the nanoparticle surface. Consequently, we propose transient exposure of reactive silver sites via localized reorganization rather than total removal of the starch shell.

References

1- H. Pohl, M. Mumtaz, *Regul. Toxicol. Pharma*col. 132 (2022) 105187.

2-Salahaddin Hajizadeh, Khalil Farhadi, Mehrdad Fororugh and Reza Emamali Sabzi, Silver nanoparticle as a cyanide colorimetric sensor in aqueous media. *Analytical Methods* 3 (2011) 2599.

3-EPA. United States. Environmental Protection Agency Clarification of Free and Total Cyanide Analysis for Safe Drinking Water Act (SDWA) Compliance. EPA 815-B-20-004 June 2020.

4- USEPA Document. "Testing for Cyanide in Drinking Water" Michael F. Delaney, Ph.D. Director of Laboratory Services Operations Division, Massachusetts Water Resources Authority (MWRA)-March 2017.

5- Chromium in drinking-water Background document for development of WHO Guidelines for drinking-water quality. *World Health Organization 2020* .WHO/HEP/ECH/WSH/2020.3.

6- Amirmostafa Amirjani, Farzad Firouzi, Davoud Fatmehsari Haghshenas. Predicting the Size of Silver Nanoparticles from Their Optical Properties. *Plasmonics* 15 (2020) 1077-1082.

7- Muhammad Ismail, M.I. Khan, Kalsoom Akhtar, Murad Ali Khan, Abdullah M. Asiri, Sher Bahadar Khan. Biosynthesis of silver nanoparticles: A colorimetric optical sensor for detection of hexavalent chromium and ammonia in aqueous solution. *Physica E: Low-dimensional Systems and Nanostructures* 103 (2018) 367-376.

8- S. Izadi, J. Tashkhourian, S. A. Hosseini Hafshejani. Biosynthesized silver nanoparticles base on bittter orange bloom extract and its application for the determination of cyanide ion in environmental samples. *J.Photochem.& Photobiology,A:Chemistry* 446 (2024) 115173.

9-Rafael Eleodoro De Góes, Marcia Muller, José Luís Fabris. Spectroscopic Detection of Glyphosate in Water Assisted by Laser-Ablated Silver Nanoparticles. *Sensors* 17 (2017) 954. doi:10.3390/s17050954 .

10- R. A. Soomro, A. Nafady, S irajuddin, N. Memon, T. H. Sherazi, N. H. Kalwar. L-Cysteine protected copper nanoparticles as colorimetric sensor for mercuric ions. *Talanta* 130 (2014) 415-422.

11- Che Sulaiman, B. Chieng, M. Osman, K. Ong, J. Rashid, W. Wan Yunus, S. Noor, N. Kasim, N. Halim, A. Mohamad, A review on colorimetric methods for determination of organophosphate pesticides using gold and silver nanoparticles, *Microchim. Acta* 187 (2020) 1-22.

12-Kamlesh Shrivasa, Bhuneshwari Sahua, Manas Kanti Deba,, Santosh Singh Thakurb, Sushama Sahua, Ramsingh Kurreya, Tushar Kanta, Tarun Kumar Patlea, Rajendra Jangdec. Colorimetric and paper-based detection of lead using PVA capped silver nanoparticles: Experimental and theoretical approach. *Microchemical Journal* 150 (2019) 104156.

13-Amirmostafa Amirjani, Davoud Fatmehsari Haghshenas. Facile and on-line colorimetric detection of Hg^{2+} on localized surface Plasmon Resonance (LSPR) of Ag nanotriangles. *Talanta* 192 (2019) 418-423.
14- Wannida Sapyen, Saowanee Toonchue, Narong Praphairaksit, Apichat Imyim. Selective colorimetric detection of Cr(VI) using starch-stabilized silver nanoparticles and application for chromium speciation *Spectrochimica Acta Part A: Molecular and Biomolecular Spectroscopy* 274 (2022) 121094.
15- Aswathy Ravindrana, M. Elavarasi, T. C. Prathna, Ashok M. Raichur, N. Chandrasekarana, Amitava Mukherjeea. Selective colorimetric detection of nanomolar Cr(VI) in aqueous solutions using unmodified silver nanoparticles. *Sensors and Actuators B* 166-167 (2012) 365-371.
16- Xiaoyan Wu, Yunbo Xu, Yangjun Dong, Xue Jiang, Ningning Zhu. Colorimetric determination of hexavalent chromium with ascorbic acid capped silver nanoparticles. *Anal. Methods* 5 (2013) 560-565.
17- Qiangsheng Xue, Xin Li, Yinxian Peng, Peng Liu, Hongbing Peng, Xiangheng Niu. Polyethylenimine-stabilized silver nanoclusters act as an oxidoreductase mimic for colorimetric determination of chromium(VI). *Microchimica Acta* 187 (2020) 263.
18- Shreya Bhatt, Gaurav Vyas, Parimal Paul. Rosmarinic. Acid-Capped Silver Nanoparticles for colorimetric detection of CN^- and redox-modulated surface reaction-aided detection of Cr(VI) in water. *ACS Omega* 7 (2022) 1318-1328.
19- P. Vasileva, L. Djerahov, I. Karadjova. Raffinose Capped Silver Nanoparticles: A New Localized Surface Plasmon Resonance Based Sensor for Selective Quantification of Cr(VI) in Waste Waters. *Molecules* 26 (2021) 5418.
20 - Shunzhen He, Xi Lin,Hao Liang, Fubing Xiao, Feifei Li, Can Liu,Pengfei Fan, Shengyuan Yang and Yong Liu. Colorimetric detection of Cr(VI) using silver nanoparticles functionalized with PVP. *Anal. Methods* 11 (2019) 5819.
21- Ayça Girgin, Hilal Akbıyık, Buse Tuğba Zaman, Gülten Çetin, Sezgin Bakırdere. Colorimetric Sensor based AgNPs for the Detection of cyanide using UV-Vis Spectrophotometry. *Chemistry Europe*. *Chemistry Select* 8 (2023) e202301663.
22-Hatam Hassanvand, Payman Hashemi. Synthesis of Silver Nanoparticles -Agarose Composite and its Application to the Optical Detection of Cyanide Ion. The Japan Society for Analytical Chemistry *Analytical Science,* 34 (2018) 567-570.
23- Li Shang, Chuanjiang Qin, Lihua Jin ,Lixiang Wang, Shaojun Dong. Turn-on Fluorscent Detection of Cyanide Based on the Inner Filter Effect of Silver Nanoparticles. *Analyst* 134 (2009) 1477-1482.
24- Raveendran, Jie Fu, Scott L. Wallen. Completely "Green" Synthesis and Stabilization of Metal Nanoparticles Poovathinthodiyil. *JACS Comm*. 125 (2003) 13940-13941.
25- K. Wongravee, T. Parnklang, P. Pienpinijtham, C. Lertvachirapaiboon, Y. Ozaki, C. Thammacharoen, S. Ekgasit. Chemometric analysis of spectroscopic data on shape evolution of silver nanoparticles induced by hydrogen peroxide. *Phys. Chem. Chem. Phys*. 15, 12 (2013) 4183-4189.
26 - A. Amirjani, N. N. Koochak, D. Fatmehsari Haghshenas. Investigating the Shape and Size-Dependent Optical Properties of Silver Nanostructures Using UV–vis Spectroscopy. *J. Chem. Educ.* 96, 11 (2019) 2584-2589.
27- N. G. Bastús, Jordi Piella, Victor Puntes. Quantifying the Sensitivity of Multipolar (Dipolar, Quadrupolar, and Octapolar) Surface Plasmon Resonances in Silver Nanoparticles: The Effect of Size, Composition, and Surface Coating. *Langmuir* 32 (2016) 290-300.
28- D. W. Boukhvalov, I. S. Zhidkov, E. Z. Kurmaev, E. Fazio, S. O. Cholak, L. D'Urso. Atomic and electronic structures of stable linear carbon chains on Ag nanoparticles. *Carbon* 128 (2018) 296-301.
29 - S. Tajammul Hussain, E. M. Iqbal, M. Mazhar. Size control synthesis of starch capped-gold nanoparticles *J. Nanop. Research* 11 (2009) 383-391.
30 -F. Burriel Marti, F. Lucenna Conde, S. Arribas Jimeno, J. Hernandez Mendez. *Química Analitica Cualitativa*. Parte tercera. *Química Analítica de los Aniones.* Thompson Editors, Spain. Paraninfo, SA. 8ª ed., 2006.
31-Arnaud Sanchez-Hachair, Annette Hofmann. Hexavalent chromium quantification in solution: Comparing direct UV visible spectrometry with 1,5-diphenylcarbazide colorimetry. *Comptes Rendus Chimie* 21 (2018) 890-896.
32 - I. J. Buerge, S. J. Hug. Kinetics and pH Dependence of Chromium(VI) Reduction by Iron(II). *Environ. Sci. Technol*. 31, 5 (1997) 1426-1432.
33- J. Buerge, S. J. Hug. Influence of Organic Ligands on Chromium(VI) Reduction by Iron(II). *Environ. Sci. Technol*. 32 (1998) 2092-2099.

34 - S. J. Hug, H.-U. Laubscher, B. R. James. Iron (III) Catalyzed Photochemical Reduction of Chromium(VI) by Oxalate and Citrate in aqueous solution. *Environ. Sci. Technol*. 31, 1 (1996) 160-170.
35 -Analytical Methods Committee, Recommendations for the definition, estimation and use of the detection limit. *Analyst* 112 (1987) 199-204.
36 - J. N. Miller, J. C. Miller. Statistics and Chemometrics for Analytical Chemistry, 4th edition, Pearson Education S.A, Prentice Hall, Madrid, 2002, p. 125 Chap. 5, Section 5.7. Detection limits.
37- C. D. Montgomery, G. C. Runger. Applied Statistics and Probability for Engineers, 3rd edition, John Wiley & Sons, Inc., 2002, USA.
38- S. Paná, M. V. Marinelli, M. Bonansea, A. Ferral, D. Valente, V. Camacho Valdez, I. Petrosillo. The multiscale nexus among lands use-land cover changes and water quality in the Suquía River Basin, a semi-arid region of Argentina. *Scientific Reports* 14 (2024) 4670.
https://doi.org/10.1038/s41598-024-53604-0

39- S. Ruiz, F. Morandini, M. Panzetta, F. Lipari, M. Irrazabal, R. Toselli, M. Der Ohannesian, C. Amieva, et al., Urban wastewater overflows as hotspots for dissemination of bacteria producing extended-spectrum β-lactamases and carbapenemases in the Suquía River, Argentina. *Frontiers in Microbiology*, 16 (2025) 1669531. https://doi.org/10.3389/fmicb.2025.1669531